www.MaterialsViews.com

Organic Photovoltaic Cells: From Performance Improvement to Manufacturing Processes

Hongseok Youn, Hui Joon Park, and L. Jay Guo**

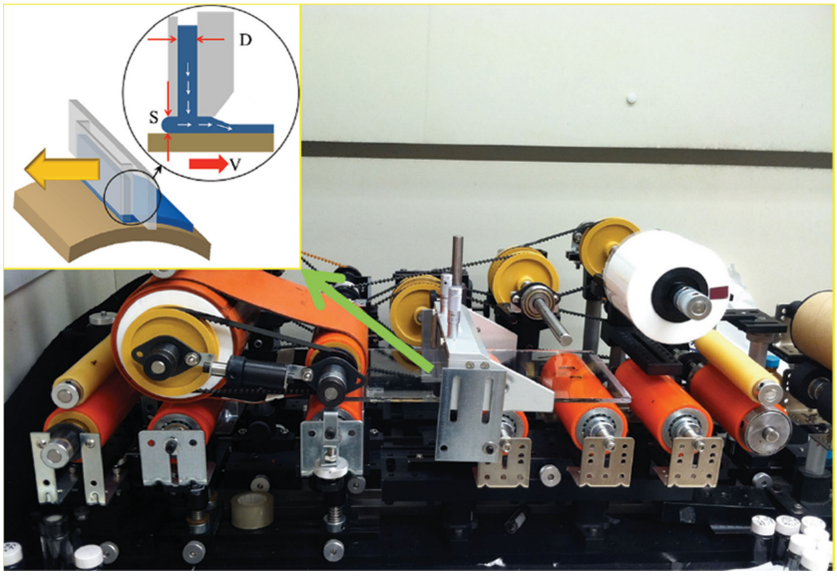

From the Contents

Organic photovoltaics (OPVs) have been pursued as a next generation power source due to their light weight, thin, flexible, and simple fabrication advantages. Improvements in OPV efficiency have attracted great attention in the past decade. Because the functional layers in OPVs can be dissolved in common solvents, they can be manufactured by eco-friendly and scalable printing or coating technologies. In this review article, the focus is on recent efforts to control nanomorphologies of photoactive layer and discussion of various solution-processed charge transport and extraction materials, to maximize the performance of OPV cells. Next, recent works on printing and coating technologies for OPVs to realize solution processing are reviewed. The review concludes with a discussion of recent advances in the development of non-traditional lamination and transfer method towards highly efficient and fully solution-processed OPV.

1. Introduction

With the rapid development of modern technologies, flexible electronic devices have drawn much interest in recent years.[1,2] Since flexible devices can be bent, folded, light weight, and portable, it is expected that they may significantly extend the scope of present electronic devices. Especially, if the flexible photovoltaic (PV) cells, based on organic or other thin film semiconductors, can be realized, new opportunities that can help to address our energy crises exist, such as building integrated PV applications, energy sources of flexible portable devices, etc.

To realize the future possibilities, the power conversion efficiency (PCE) of organic photovoltaic (OPV) cells should be improved, and effective manufacturing processes, which can not only scale up the laboratory-scale devices to large area format without sacrificing performances but also minimize the manufacturing cost, need to be developed. In this review article, we will focus the recent efforts to achieve these goals. Firstly, approaches to control nanomorphologies of organic semiconductor photoactive layer, which are directly related to the performance of OPV cells, will be discussed, and the importances of solution-processed charge transport and extraction materials, affecting the charge collection property of OPV cells, will be studied. Next, we will move to the recent works about printing and coating technologies for OPVs to realize solution processed OPV. In the last section, we will discuss non-traditional lamination and transfer method for the OPV cell fabrication.

2. Nanomorphologies in Photoactive Layers

One of the most essential layers of OPV cells is the photoactive layer, which converts the photons to free charge carriers. Especially, nanomorphologies of organic semiconductors in photoactive layer play crucial roles in exciton generation, diffusion and dissociation as well as charge transport and recombination. In this section we review the recent efforts to control the nanostructures of photoactive layer to maximize the performance of OPV cells.

2.1. Bulk Heterojunctions

In OPV cells, photogenerated negative and positive charges, which form excitons, are tightly bound each other due to the strong Coulombic attraction, resulted from the low dielectric constants in organic semiconductors, therefore additional force is required for those excitons to be dissociated to free charge carriers, consequently contributing photocurrent of PV cells, before recombination.[3–7] The most successful approach until now is by forming heterojunction interface between an electron-donor (donor) and an electron-acceptor (acceptor) material with sufficient energy level offset between the two that can induce ultrafast electron transfer. In this architecture, the excitons, diffused to the interface, can be efficiently dissociated into free charge carriers through the charge transfer state. However, the limited diffusion distance of excitons in organic semiconductor, known to be around 10 nm-scale, is mismatched to the thickness of photoactive layer for efficient photon absorption, usually over 100 nm,[8–15] therefore further strategy is necessary to improve the exciton dissociation efficiency.

Bulk heterojunctions (BHJs), composed of interpenetrating nanoscale networks of donor and acceptor, is one of the most widely studied structures in OPV cell researches since their first reports.[16–18] Because their domain sizes are on the order of the exciton diffusion length, giving large interfacial areas between the domains, the dissociation of excitons can be facilitated at the domain interface. However, due to the random nature of the structure, optimizing the complex morphology to form effective pathways in order for the dissociated charges to reach each electrode, as well as large interfacial areas, has been one of the most crucial issues in the achievement of high efficiency OPV cells using BHJ structures.

BHJ nanostructure can be easily fabricated by blending the donor with acceptor materials. To optimize BHJ blend, various approaches have been developed for last decades. Among them, solvent additive techniques, thermal annealing and solvent annealing are the most successful approaches that can significantly affect the nanomorphologies of BHJ blend. Solvent additives are commonly added to the blend solution before spin-casting to improve the performance of BHJ PV cells. For example, octanedithiol (ODT) in poly[2,6-(4,4-bis-(2-ethylhexyl)-4H-cyclopenta[2,1-b;3,4-b′]dithiophene)-alt-4,7-(2,1,3-benzothiadiazole)] (PCPDTBT):[6,6]-phenyl C_{71}-butyric acid methyl ester ($PC_{71}BM$) blend system, which is selectively soluble to fullerene derivative and has higher boiling point than the host solvent such as chlorobenzene, can increase the crystallinity and the degree of intermixing of components, as studied by atomic force microscopy (AFM), transmission electron microscopy (TEM), grazing incidence wide angle X-ray scattering (GIWAXS), and nuclear magnetic resonance (NMR).[19–22] **Figure 1**a and b show the morphological change of PCPDTBT:$PC_{71}BM$ blend without and with ODT. Furthermore, 1-chloronaphthalene (CN) in poly[(4,4-didodecyldithieno[3,2-b:2′,3′-d]silole)-2,6-diyl-alt-(2,1,3-benzothiadiazole)-4,7-diyl] (Si-PDTBT):$PC_{71}BM$ blend system[23] and diiodooctane (DIO) in poly[[4,8-bis[(2-ethylhexyl)oxy]benzo[1,2-b:4,5-b′]dithiophene-2,6-diyl][3-fluoro-2-[(2-ethylhexyl)carbonyl]thieno[3,4-b]thiophenediyl]]

Dr. H. Youn[+]
National Center for Nanoprocess and Equipment
Korea Institute of Industrial Technology (KITECH)
Gwangju 500–480, Korea
Prof. H. J. Park
Division of Energy Systems Research
Ajou University
Suwon 443–749, Korea
E-mail: huijoon@ajou.ac.kr
Prof. L. J. Guo
Department of Electrical Engineering and Computer Science
The University of Michigan
Ann Arbor 48109, USA
E-mail: guo@umich.edu
[+]Present Address: Department of Mechanical Engineering, Hanbat National University 125 Dongseodaero, Yuseong-gu, Daejeon, 305-719, South Korea

DOI: 10.1002/smll.201402883

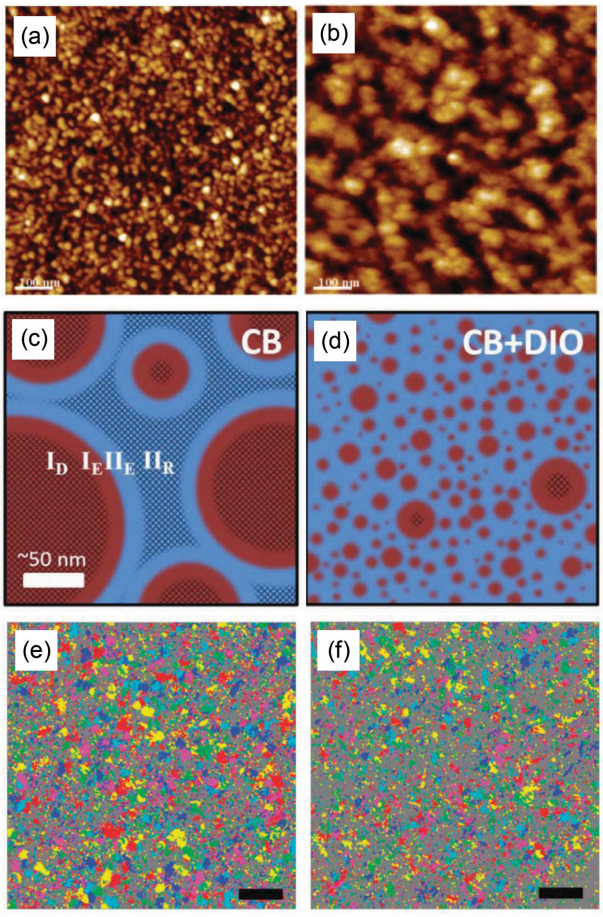

Figure 1. (a,b) AFM images of BHJ films cast from PCPDTBT:$PC_{71}BM$ (exposed PCPDTBT networks after removal of $PC_{71}BM$) (a) without and (b) with 1,8-octanedithiol. Reproduced with permission.[20] Copyright 2008, American Chemical Society. (c,d) Morphological schematic of PTB7:$PC_{71}BM$ BHJ films cast by (c) chlorobenzene (CB) and (d) CB + DIO. Region I (red) is the pure PCBM agglomerate phase and Region II (blue) is the mixed matrix phase. Regions I_E and II_E are those where the photovoltaic effect is most efficient. Region I_D is a region that is dead due to exciton relaxation and Region II_R is where geminate recombination is high. Reproduced with permission.[24] Copyright 2013, Wiley. (e,f) TEM images of $(DTS(PTTh_2)_2)$:$PC_{71}BM$ BHJ film: lower magnification, false colour images encoding the direction and size of crystalline regions for BHJ films cast from a pure solvent (e) and addition of 0.25% v/v DIO solvent additive (f). A reduction in the length scale is observed with the 0.25% v/v DIO solvent additive. Scale bars, 100 nm. Reproduced with permission.[26] Copyright 2012, Macmillan Publishers Ltd.

Hongseok Youn received his B.S. degree in mechanical engineering in Korea University, Korea, in 2001. He received M.S. and Ph.D. degrees in mechanical engineering at the Korea Advanced Institute of Science and Technology in 2005 and 2011, respectively. From 2011 to 2014, he was a post doctoral researcher in electrical engineering and computer science at the University of Michigan, Ann Arbor, USA. After completing this post doctoral research, he has joined the National Center for Nanoprocess and Equipment, Korea Institute of Industrial Technology (KITECH), as a Senior Researcher.

Hui Joon Park received his B.S. and M.S. degrees in materials science and engineering from Seoul National University, Korea, in 2002 and 2004, respectively. From 2004 to 2006, he was with LG Electronics as a Research Engineer. From 2006 to 2007, he was a Research Scientist at the Korea Institute of Science and Technology, Korea. He received a Ph.D. in organic electronics and nanofabrication at the University of Michigan, Ann Arbor, USA, in 2012. After completing his Ph.D., he became a Senior Research Engineer at the Intel Corporation, USA, from 2012 to 2014. Since 2014, he has been in the Division of Energy Systems Research, Ajou University, Korea, where he is currently Assistant Professor.

L. Jay Guo is a professor of Electrical Engineering and Computer Science at the University of Michigan, with joint appointments in Mechanical Engineering, Macromolecular Science and Engineering, and Applied Physics. His group's research includes polymer-based photonic devices and sensor applications, organic photovoltaics, plasmonic nanophotonics/metamaterials, and nanoimprint-based and roll-to-roll nanomanufacturing technologies. He received his Ph.D. in Electrical Engineering from the University of Minnesota in 1997.

(PTB7):$PC_{71}BM$ blend system[24,25] helps to disperse fullerene aggregates, giving rise to better phase separation (Figure 1c and 1d). DIO can be also applied to solution-processable small molecular system such as 5,5′-bis[[4-(7-hexylthiophene-2-yl)thiophene-2-yl]-[1,2,5]thiadiazolo[3,4-c]pyridin]-3,3′-di-2-ethylhexylsilylene-2,2′-bithiophene ($DTS(PTTh_2)_2$): $PC_{71}BM$ blend. In this system, domain size can be reduced from 20–30 nm to 15–20 nm, using DIO as solvent additive (Figure 1e,f).[26] Consequently, solvent additive can be utilized to improve the crystallinity or to decrease size of nano-domains of BHJ blend. However, proper additives should be selected after considering the properties of blend systems.

Thermal and solvent annealing have been widely studied methods to optimize BHJ nanomorphologies. Especially, their effects on the morphologies of a model OPV system made of donor material poly(3-hexylthiophene-2,5-diyl) (P3HT) and acceptor material phenyl-C_{61}-butyric acid methyl ester (PCBM) blend are extensively investigated by various characterization methods such as, AFM, TEM, GIWAXS, dynamic secondary ion mass spectrometry (DSIMS), X-ray photoelectron spectroscopy (XPS), etc. After thermal treatment, known as thermal annealing, crystallinity and degree of intermixing of components can be significantly improved, giving better device performances.[27,28] For example, **Figure 2** shows 2D GIWAXS results of neat P3HT, neat PCBM, and blends with P3HT:PCBM blending

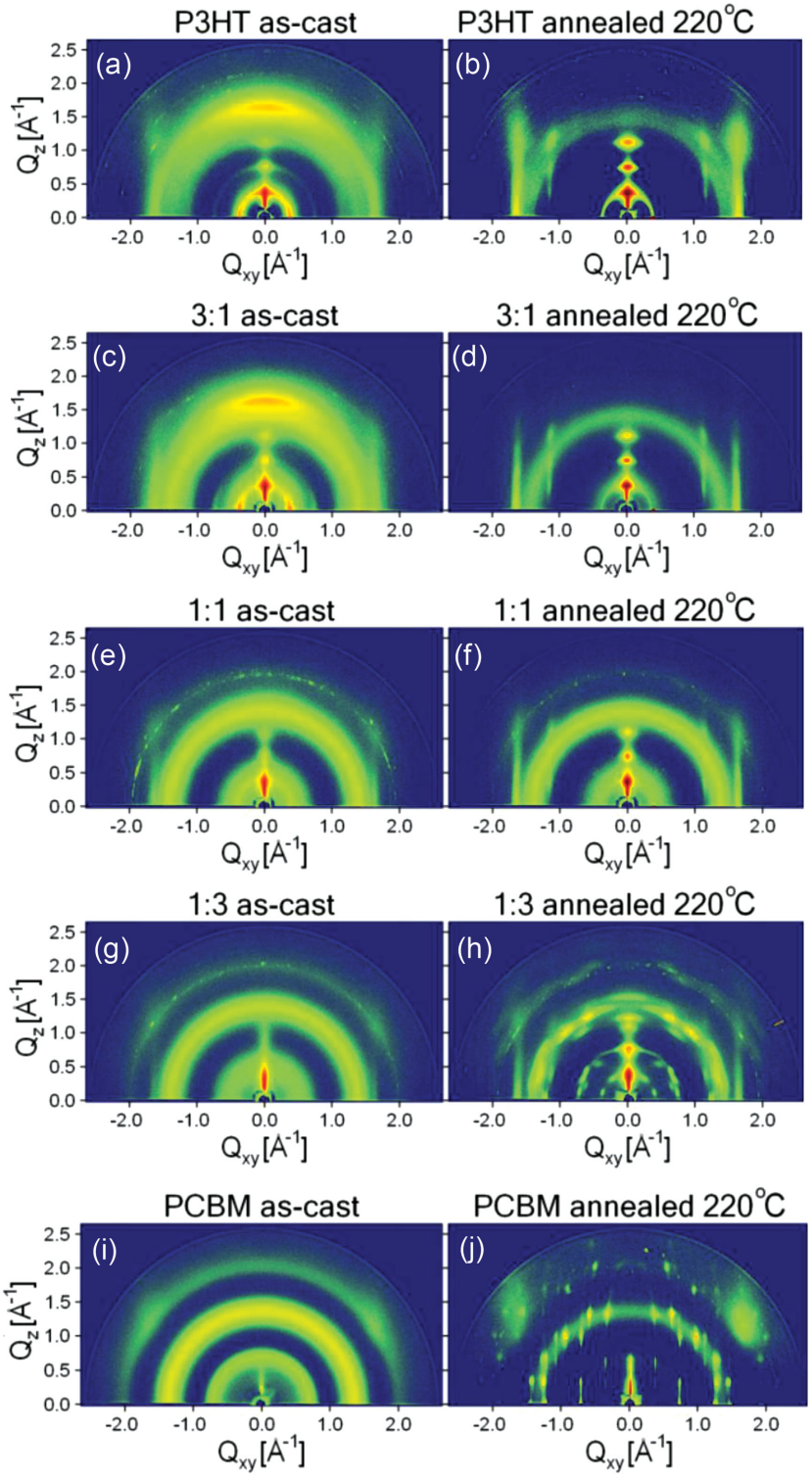

Figure 2. 2D GIWAXS images of (a) as-cast P3HT, (b) P3HT annealed at 220 °C, (c) as-cast 3:1 P3HT:PCBM blend, (d) 3:1 P3HT:PCBM blend annealed at 220 °C, (e) as-cast 1:1 P3HT:PCBM blend, (f) 1:1 P3HT:PCBM blend annealed at 220 °C, (g) as-cast 1:3 P3HT:PCBM blend, (h) 1:3 P3HT:PCBM blend annealed at 220 °C, (i) as-cast PCBM, and (j) PCBM annealed at 220 °C. Reproduced with permission.[27] Copyright 2010, Wiley.

ratios 3:1, 1:1 and 1:3 both as-cast and after thermal annealing at 220 °C.[27] For each thin film composition, significant morphological rearrangements were observed after thermal annealing. Nanomorphologies of BHJ blends can be also optimized by controlling solvent evaporation rate during the casting of blend film, known as solvent annealing.[29–32] As shown in **Figure 3**, molecular ordering such as nucleation of well-aligned P3HT crystallites and aggregation of PCBM during the drying of P3HT:PCBM blend were characterized using in-situ GIWAXS and laser reflectometry.[29] In addition to aforementioned extrinsic routes such as annealing based-processes to improve BHJ film morphologies of photoactive layers, intrinsic strategies such as adjusting the molecular structures have also been successfully employed to optimize the BHJ morphologies of photoactive layer, eventually improving the OPV device performances.[33–35]

Besides solvent additive approaches and the annealing-based processes to facilitate the spontaneous phase separation of components, advanced processes to help molecules to have preferred organization with additional forces also have been developed. For instance, gas-permeable polydimethylsiloxane (PDMS) cover layer can be utilized to prevent the component of blend having lower surface energy from migrating to the top surface during film casting, which can induce more uniform vertical distribution of components (**Figure 4**). In this process, because a shear stress applied to the polymer solution, which causes organization of the polymer-across the entire depth between two plates, is much more effective than that between a plate and an air surface, highly crystallized polymer domains, of which the crystallinity is higher than the thermal-annealed for tens of minutes and compatible to the solvent-annealed for several hours, could be achieved within a few seconds without annealing.[36,37] More uniform distribution and higher crystallinity of the components, which are favorable for charge generation and transportation and cannot be achieved by conventional thermal annealing and solvent annealing methods, give improved the performances of PV cells.

2.2. Bilayer-Based Structures

The bilayer donor and acceptor heterojunction for OPV, pioneered by Tang in 1986,[38] is a simple planar structure that has an advantage of easy optimization of devices and the efficient free charge carrier transportation. This type of structure has been exploited especially for small molecule-based OPV

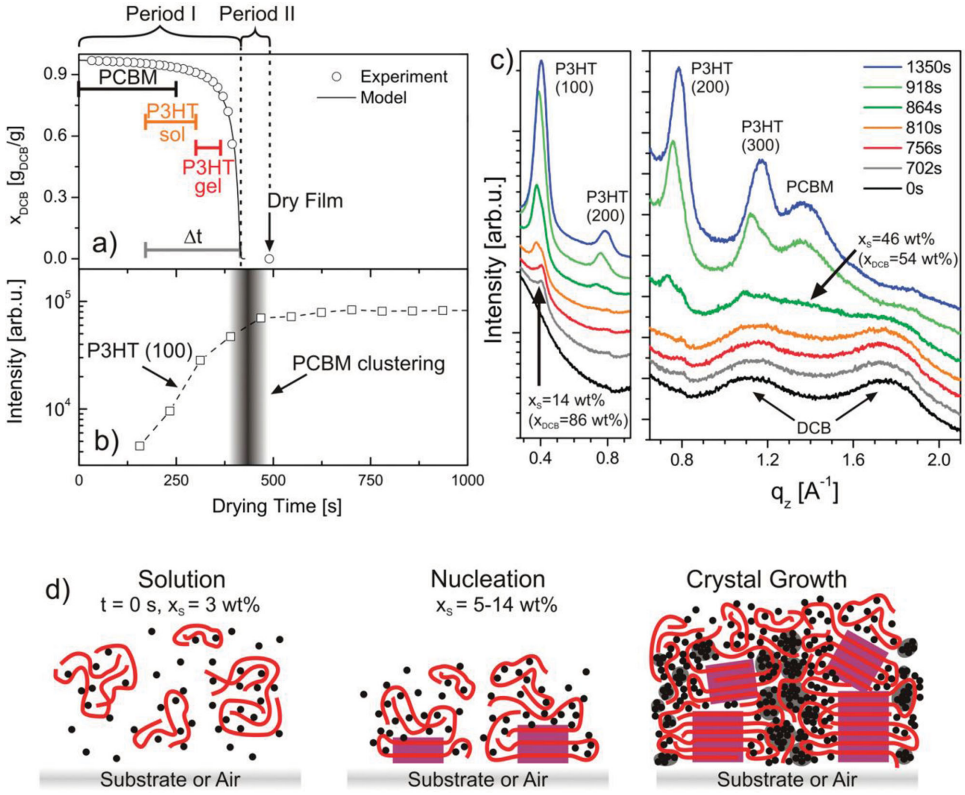

Figure 3. (a) Evolution of film composition (solvent mass fraction x_{DCB}) during film drying of P3HT:PCBM films on PEDOT:PSS/glass as obtained from laser reflectometry (data, symbols; fit from model, line). The labeled bars indicate ranges of phase transitions as expected from the superposition of the binary phase diagrams. Two different drying phases are marked as period I (constant rate period) and period II (falling rate period). Period II is determined experimentally from the time period between last interference peak and a constant reflectometer signal. The constant rate period time after crossing P3HT solubility is denoted as Δt. (b) To obtain the measure of overall P3HT crystallinity in the blend film, the integrated area of the P3HT (100) Bragg peak is plotted versus drying time. (c) Selected profile plots at increasing drying times showing the emergence of the diffraction peaks of PCBM, P3HT (h00) Bragg peaks and disappearance of the diffraction peaks of the evaporating solvent DCB on a silicon dioxide/silicon substrate (log scale left, linear right). These were the only measurements not carried out on PEDOT:PSS. (d) Scheme shows the stages of molecular arrangement during solvent evaporation with nucleation at the substrate or air interface. Lines represent P3HT chains, purple squares are crystalline P3HT domains, and dots are PCBM molecules. Reproduced with permission.[29] Copyright 2011, American Chemical Society.

devices. However, restricted photo-carriers generation due to short exciton diffusion length and the limited interfacial areas between the donor and acceptor domains responsible for the charge separation made this structure be left behind predominantly investigated BHJ structure. However, Treat et al. showed that PCBM acceptor, added on top of P3HT donor layer by float-casting, can efficiently diffuse into P3HT layer during thermal annealing, resulting in a homogeneously mixed system.[39] Moreover, they found that the interdiffusion of PCBM into P3HT takes place in the disordered phase of P3HT without affecting the crystalline structure of P3HT (**Figure 5**). This indicates that interfacial area of simple bilayer structure can be significantly increased by improving the intermixing between donor and acceptor and, therefore, it may be possible to utilize this type of structure as an efficient photoactive layer of OPV cells, different from the stereotype BHJ structure. This concept was further proven by the works of Chen et al. and Lee et al.,[40,41] who independently demonstrated that bilayer-based structure could intimate the BHJ structure by solution casting of PCBM on P3HT layer using orthogonal solvent such as dichloromethane (DCM), followed by thermal annealing to increase the intermixing of donor and acceptor. PCEs comparable to those of BHJ-based PV cells have been achieved (**Figure 6**a). However, to maximize the intermixing of donor and acceptor phases, only tens of nanometers thin donor layer was used, not proper to efficient light harvesting. Thus, the performances could not exceed those of conventional BHJ-based devices.

Recently, bilayer-based polymer PV cells superior than BHJ was demonstrated by Park et al. using two steps consecutive printing process.[42] In this process, the first printing process forms highly crystallized P3HT nanowires, which cannot be achieved by spin-casting, and the second printing process is utilized to maximize the interdiffusion of PCBM into P3HT donor phase by increasing solvent dwelling time of DCM. Figure 6c shows AFM results of high crystalline donor phase from first printing process, and DSIMS shows that the amount of diffused PCBM by second printing process is about three times higher than that by spin-casting (Figure 6e,f). Their process was valid for even 350 nm thick donor layer, which is sufficient to light absorption, resulting in about 50% improved short circuit current compared to BHJ structure. Moreover internal quantum efficiency of their PV cells was approaching 100% at certain spectral range, indicating donor-acceptor heterojunction nanostructures are optimized.

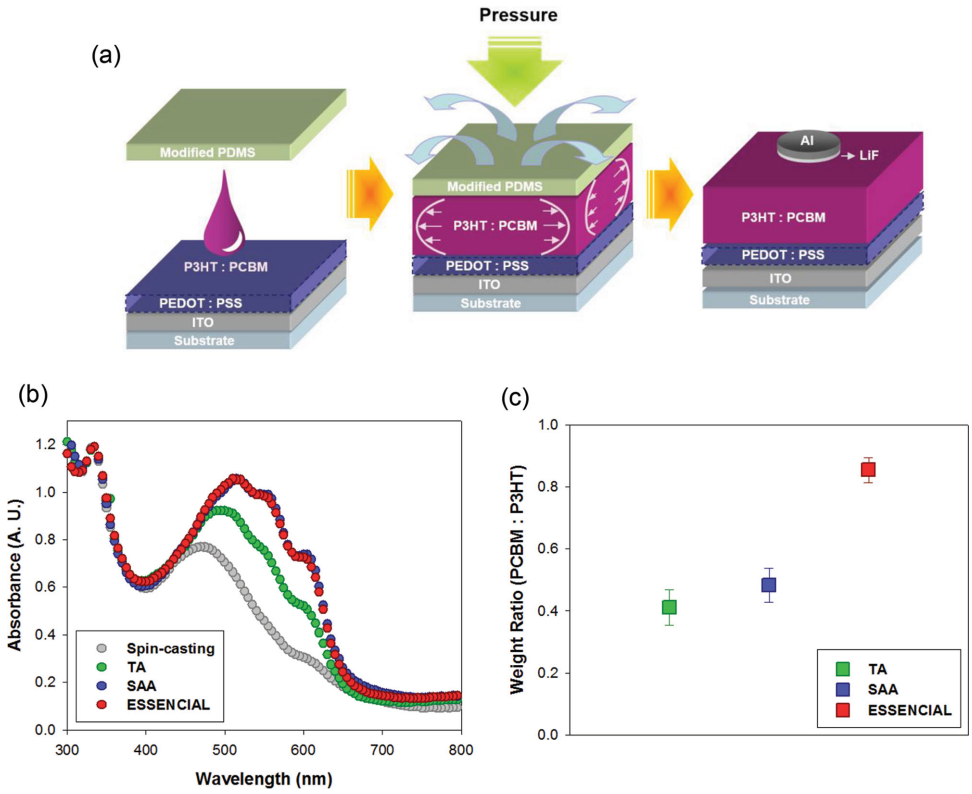

Figure 4. (a) Schematic of the process for fabricating polymer PV cells utilizing ESSENCIAL process: 1) applying blend solution (PDMS and ITO refer to polydimethylsiloxane and indium tin oxide, respectively); 2) active layer formation during solvent evaporation under pressure; and 3) isolated island-type electrode deposition on top of polymer blend film after removing the PDMS stamp. Note that the PEDOT:PSS layer is not indispensable to this processing (b) Absorption spectra of the blend films; the spectra have been normalized to the PCBM peak around 325 nm. (c) Weight ratio of PCBM to P3HT calculated by XPS results for different processing methods; the error bars represent standard deviations. Blend films cast by ESSENCIAL show better vertical uniformity approaching 1:1 weight ratio. Reproduced with permission.[36] Copyright 2010, Wiley.

In addition to P3HT:PCBM blend system, bilayer-based approach, which utilized other blend system such as poly[*N*-9″-hepta-decanyl-2,7-carbazole-alt-5,5-(4′,7′-di-2-thienyl-2′,1′,3′-benzothiadiazole)] (PCDTBT):$PC_{71}BM$ blend system, was also demonstrated.[43] By sequentially spin-casting $PC_{71}BM$, dissolved in a mixed solvent of chlorobenzene (CB)/dichlorobenzene (DCB) cosolvent and DCM, on PCDTBT layer, they could improve the interdiffusion of $PC_{71}BM$ into PCDTBT layer, giving comparable PCEs to those of conventional BHJ PV cells (Figure 6b). Consequently, by selecting proper solvent or processing that can maximize the intermixing between donor and acceptor, sequential bilayer-like heterojunction approach can be a promising candidate to high performance OPV cells.

3. Solution-Processed Materials and Printing/Coating Technologies

Soution-based manufacturing process is a decisive factor to realize scalable and low-cost OPVs. In addition, the scopes of the solution processable materials should be expanded to satisfy the practical manufacturing requirements. First of all, the materials should be dissolved into common organic solvents, and preferrably halogen-free solvent for environmental safety. Second, preferably the materials are stable enough to be handled in air conditions to reduce the manufacturing cost. However, the hole transport/extraction layers and electron extraction layers commonly used in OPV structure are mostly deposited by evaporation in the vacuum chamber, which not only requires long evacuation time and costly equipment with low material utilization, but also is not fully compatible with the solution process for making the OPVs. Therefore, advances in solution proccessable charge transport materials that can meet the practical manufacturing requirements without sacrificing performances are needed to realize scalable and efficient OPVs. This section deals with the solution processable charge transport/extraction materials.

3.1. Hole Transport/Extraction Materials: Transition Metal Oxides (WO_3, MoO_3, V_2O_5)

Though conductive poly(3,4-ehylenedioxythiophene):poly (styrenesulfonate) (PEDOT:PSS) is commonly used as hole transporting layer and has good printability, but it is considered as a source of device degradation due to its water-born and acidic nature, which seriously impacts the long-term stability of the OPV devices.[44,45]

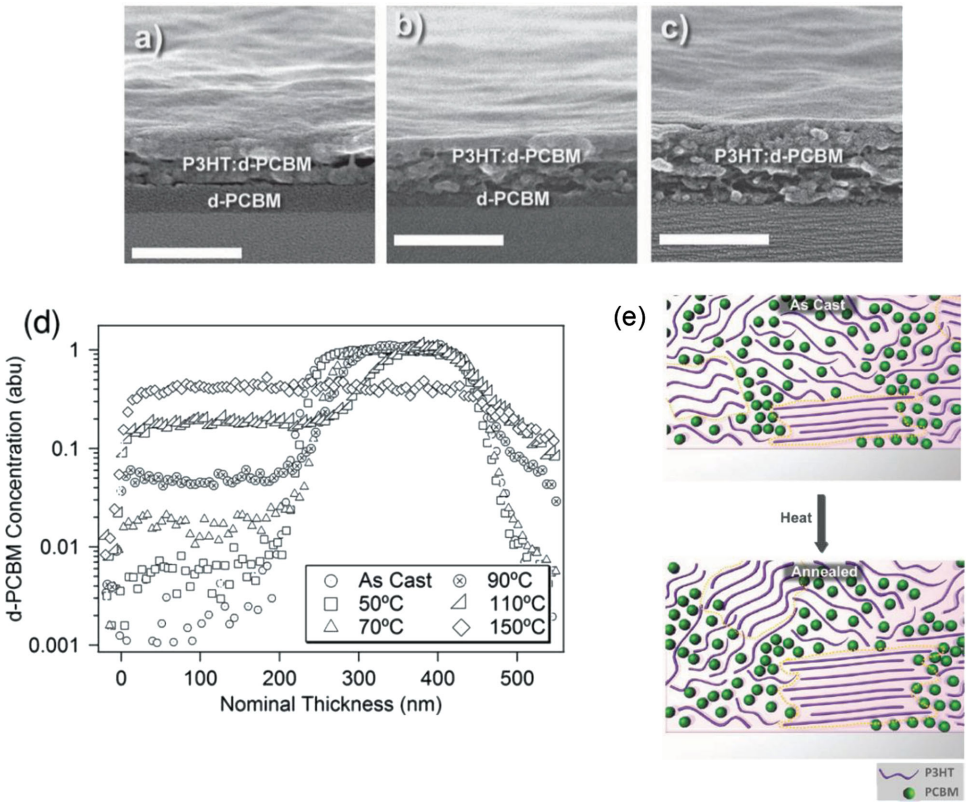

Figure 5. Cross sectional SEM images of a P3HT/d-PCBM bilayer on a silicon wafer annealed at (a) 70 °C, (b) 110 °C, and (c) 150 °C for 5 min. The scale bar represents a distance of 200 nm. (d) DSIMS profiles of ^2H in bilayer samples of P3HT and d-PCBM annealed from 5 minutes at different temperatures. The thicknesses of the films (which differed slightly across samples) were normalized such that 0 nm is the free surface of the film and 450 nm is the substrate. The deuterium concentrations were normalized such that the area under the counts versus distance for all profiles was the same after setting the normalized concentration in the d-PCBM part of the initial bilayer equal to 1. (e) Schematic representation of the evolution of the P3HT:PCBM BHJ morphology upon thermal annealing. Crystalline domains of P3HT are surrounded by the yellow dotted lines. It is also believed that the PCBM is distributed within the disordered P3HT regions even after thermal annealing. Reproduced with permission.[39] Copyright 2011, Wiley.

Transition metal oxides such as MoO_3,[46–49] WO_3[50–53] and V_2O_5[54,55] are widely used not only in OPVs but also in OLEDs as hole transport/extraction materials. These materials are commonly deposited by the evaporation process such as thermal evaporation and sputtering. Recently, solution processable and air stable nanoparticle based transition metal oxides have been studied extensively.[56–66] There are many ways to create transition metal oxide film via solution process, which are divided into nanoparticle approaches,[56–62] hydrolysis and sol-gel methods.[51,63–66] As a nanoparticle approach, the MoO_3 nanoparticle suspension (MoO_3 nanoparticles dispersed in solvents) can be utilized to form hole transport layer by spin-casting and OPVs, fabricated using this layer, give improved the shunt resistance, compared to the conventional PEDOT:PSS-based OPVs as summarized in **Table 1**. The fill factor of the device coated by MoO_3 nanoparticle suspension was also comparable to those made using PEDOT:PSS. Even though there are optical losses in the thick MoO_3 layer, they are valuable in the scalable devices preventing the shunt issue. As for hydrolysis cases, to synthesize V_2O_5, typically the vanadium (III) acetylacetate ($V(C_5H_7O_2)_3$) is dissolved into methanol and

Table 1. Performances of the OPV devices with different solution-based transition metal oxides.

Structure Active Materials	HTL	V_{oc} [V]	J_{sc} [mA/cm^2]	FF [%]	PCE [%]	R_sc) [Ω cm^2]	R_pd) [Ω cm^2]	Ref.
Norm.[a)] P3HT:PCBM	PEDOT:PSS	0.56	7.81	57.4	2.53	0.8	14 k	[55]
Norm.[a)] P3HT:PCBM	MoO_3 (47 nm)	0.56	7.61	58.0	2.47	1.1	107 k	
Inverted[b)] P3HT: PCBM	PEDOT:PSS	0.58	8.7	64.7	3.2	0.9	568 k	[51]
Inverted[b)] P3HT: PCBM	WO_3 (60 nm)	0.58	8.1	56.7	2.70	1.9	1106 k	
Inverted[b)] P3HT:PCBM	PEDOT:PSS	0.57	10.40	66.0	3.80	3.5	1226	[54]
Inverted[b)] P3HT:PCBM	V_2O_5 (25 nm)	0.57	10.10	67.0	3.90	5.0	996	

[a)]Normal structure: ITO/HTL/Active layer/Al; [b)]Inverted structure: ITO/ETL/Active layer/HTL/Ag; [c)]Series resistance; [d)]Shunt resistance.

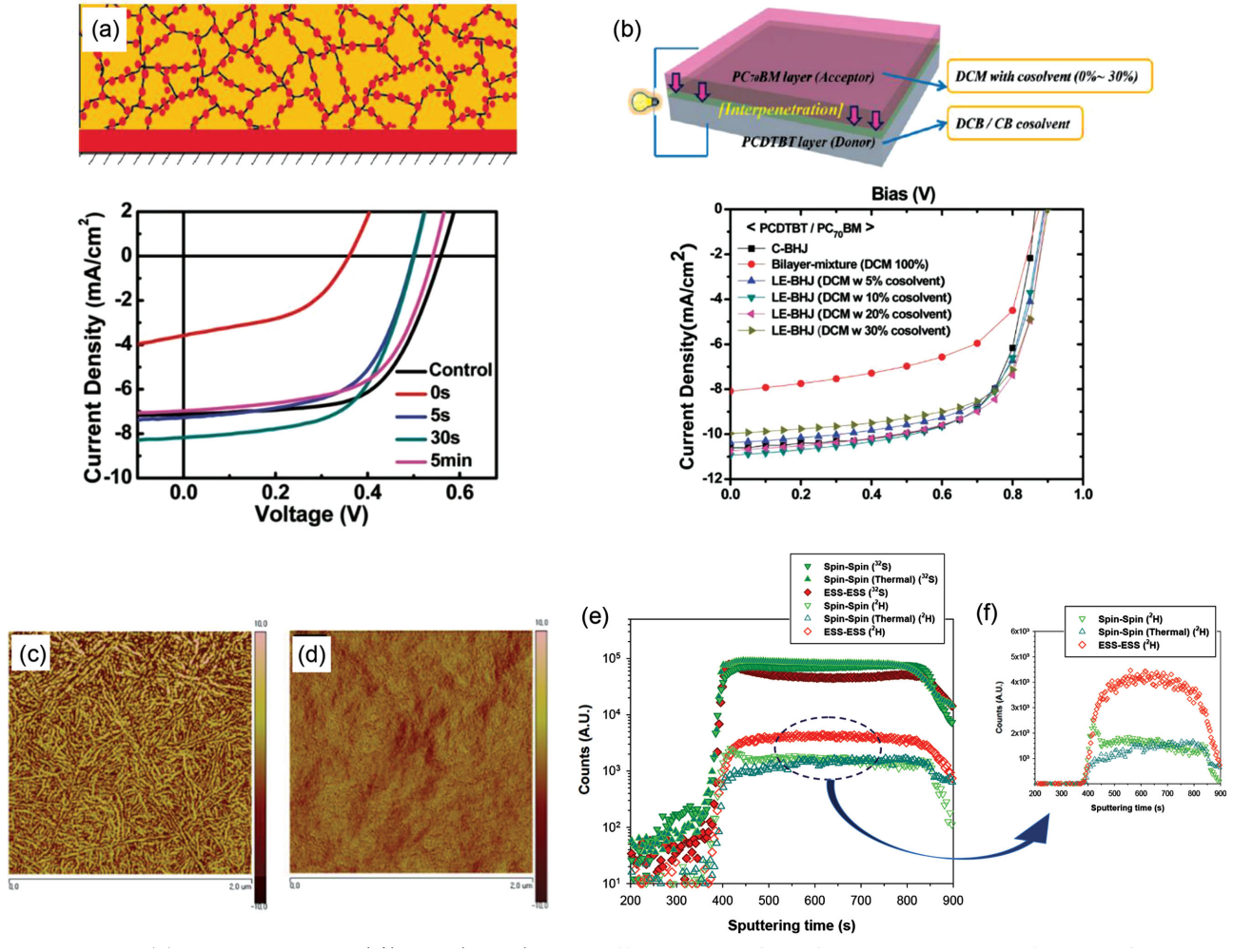

Figure 6. (a) P3HT:PCBM bilayer-based PV cells: PCBM is spin-cast on P3HT layer using DCM (P3HT is also spin-cast and thermally annealed). PCBM diffuses into P3HT film through the P3HT amorphous domains. Control device is BHJ PV cell and times in plots are annealing time for bilayer PV cells. Reproduced with permission.[40] Copyright 2011, American Chemical Society. (b) PCDTBT:$PC_{71}BM$ bilayer-based PV cells: $PC_{71}BM$ is spin-cast on PCDTBT using solvent mixtures (dissolved with various ratios of a DCB/CB cosolvent in a DCM solvent), *J–V* curves of devices made of the PCDTBT:$PC_{71}BM$ conventional (C)-BHJ, bilayer mixture (100 wt% DCM without cosolvent), and LE-BHJ (0–30 wt% cosolvent). Reproduced with permission.[43] Copyright 2011, American Chemical Society. (c)-(f) P3HT:PCBM bilayer-based PV cells fabricated by two steps consecutive printing processes: PCBM is cast on P3HT layer by printing process (P3HT is also cast by printing process and not thermally annealed), AFM phase images of P3HT nanodomains fabricated by printing process (c) and those by spin-casting followed by thermal annealing (d); DSIMS results of photoactive layers composed of P3HT and deuterated PCBM (e, f). Reproduced with permission.[42] Copyright 2013, Wiley.

potassium hydroxide is added for hydrolysis. The nanoparticles are collected by centrifuge and then redistributed into organic solvents such as ethanol and 1-butanol. This method is also very popular for the synthesis of the metal oxide nanoparticles such as ZnO nanoparticle.[67] To create V_2O_5 films by sol-gel synthesis, the starting material is vanadium (V) oxitriisopropoxide which can be dissolved into isopropanol. This solution was spin-coated on the substrate and subsequently annealed on hotplate for hydrolysis. During the annealing process, the precursor solution changes to gel and metal oxide film.[65] To synthesize WO_3, sodium tungstate (Na_2WO_4) was dissolved in deionized water and then the sodium ions were exchanged by a protonated cation exchange resin. The tungstic acid solution was diluted with isopropyl alcohol in order to coat a wet film. The resulting thin layer was baked at 200 °C to convert the tungstic acid to WO_3.[68] The performances of OPVs, based on various solution-based transition metal oxides, are summarized in Table 1. Because introducing transition metal oxide layer on the polymer active layer by solution-based processes may induce the penetration and thermal damage issues (e.g. the penetration depth of the V is around 100 nm,[66] these issues should be carefully considered during the practical solution process. In particular, not only the transition metal oxide but also graphene and graphene oxide used as hole transport materials for flexible organic solar cells.[69] In addition, solution-processed NiO was reported as one of the good materials for hole extractions, which was done by So et al.[70]

3.2. Electron Transport/ Extraction Materials

3.2.1. Metal Oxide (TiO_2, ZnO)

Solution processable TiO_2 and ZnO are widely used as an electron transport and hole blocking layers. Recently, sol-gel or nanoparticle-based materials are most commonly employed in OPVs.[71–74] The ZnO nanoparticle has excellent electron transport behavior because it has favorable electron mobility and the LUMO (lowest unoccupied molecular orbital) level is nicely matched with the LUMO level of the PCBM. It also has a good hole blocking behavior in the devices due to its deep HOMO (highest occupied molecular orbital) level (7.5 eV). The ZnO nanoparticles are usually synthesized from the hydrolysis reaction of the zinc acetate and potassium hydroxide in methanol. The nanoparticles (avg. 5 nm size) gathered by centrifuge and then redissolved in 1-butanol. Unlike nanoparticle based ZnO, sol-gel synthesis requires annealing process at higher temperature to remove organic components and crystalline.[75,76] Thus, nanoparticle solution is more suitable for the devices that need low temperature process and flexibility.

In the conventional device structure, LiF,[77] CsF,[78] Cs_2CO_3[79] are commonly used at the cathode to extract electron in OLEDs/OPVs. These very thin layers (around 1nm) are useful to reduce the energy barriers that hinder the electron extraction. However, these alkali-halide compounds are vulnerable to oxygen and moisture in air. Thus, they should be handled and deposited in the vacuum chamber. Moreover, because thin layers are easily affected by the surface condition of the underlying layer, they require very smooth surface to have a favorable the electron extraction behaviors. Owing to these material and fabrication issues, many researchers are focusing on replacing the ultra-thin reactive materials with the more stable and solution processable materials.

3.2.2. Polymer Surfactants (PEG)

Non-ionic polymer surfactants can be considered instead, such as PEG (polyethylene glycol) based on ethylene oxide monomer. Because the oxygen atom in ethylene oxide has lone pair electron, the polymer containing ethylene oxide can be dissolved into polar solvents and interacts with other materials. Moreover, these non-ionic surfactants are useful to create permanent interface dipole in not only OPVs devices but also OLEDs.[80–85] The interface dipole between the photo-active layer and cathode effectively reduces the electron extraction barrier in the device. It was found that the open circuit voltage (V_{oc}) have a large dependency on the molecular weight of the PEG. For example the PCE of the P3HT:PCBM device using PEG was 4.0% in OPVs and referece device (not having PEG) has 2.3% PCE in normal structured single cell as shown in **Figure 7**. Moreover, solution based PEG has a better stability than the Ca used at the cathode interface.

3.2.3. Water Soluble Polymers (PFN, PEIE)

Water soluble polymers such as PFN (poly [(9,9-bis(3-(*N*,*N*-dimethylamino)propyl)-2,7-fluorene)-alt-2,7-(9,9-dioctyl-fluorene)]) and PEIE (polyethylenimine ethoxylated) have simlar amino groups in their molecular structures as shown in **Figure 8** and **Figure 9**. These water soluble polymers do not have electrical conducting behaviors but the amino groups have electron donation properties that can facilitate good chemical interactions and form interface dipole. The inverted OPVs having a PFN photo-active polymer exhibited better performances when compared to regular devices, as well as improved ambient stability. The devices based on PFN showed better PCE than the ZnO-based devices.[86]

In particular, the PEIE exhibited molecular dipole itself, and it also favors the creation of interface dipole between various metal or metal oxides and significantly reduce the

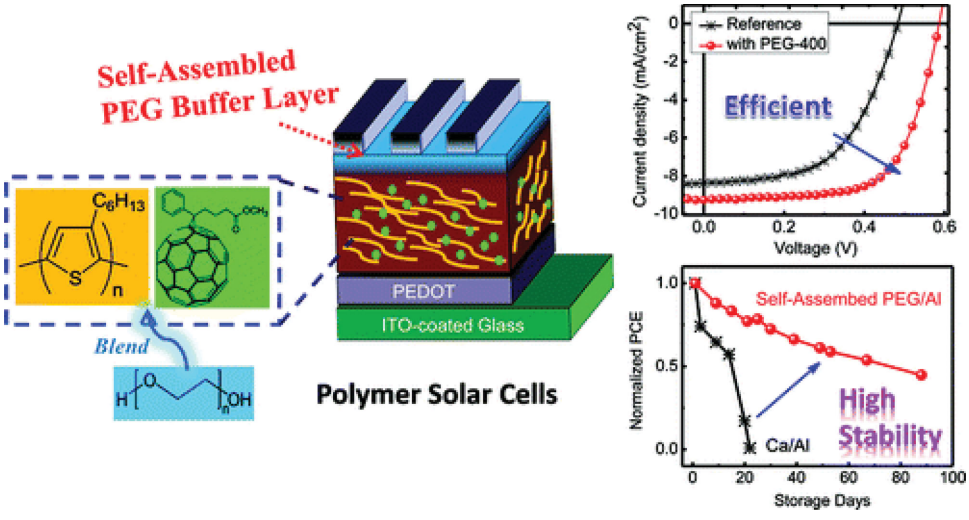

Figure 7. Schematic representation of the formation of a nanoscale PEG BL through spontaneous vertical phase separation in a polymer solar cell. Chemical structures of the materials (P3HT, PCBM, PEG) used in this study.(left) Current density–voltage (J–V) curves of devices prepared with PEG polymer and reference device. (right). Reproduced with permission.[82] Copyright 2011, American Chemical Society.

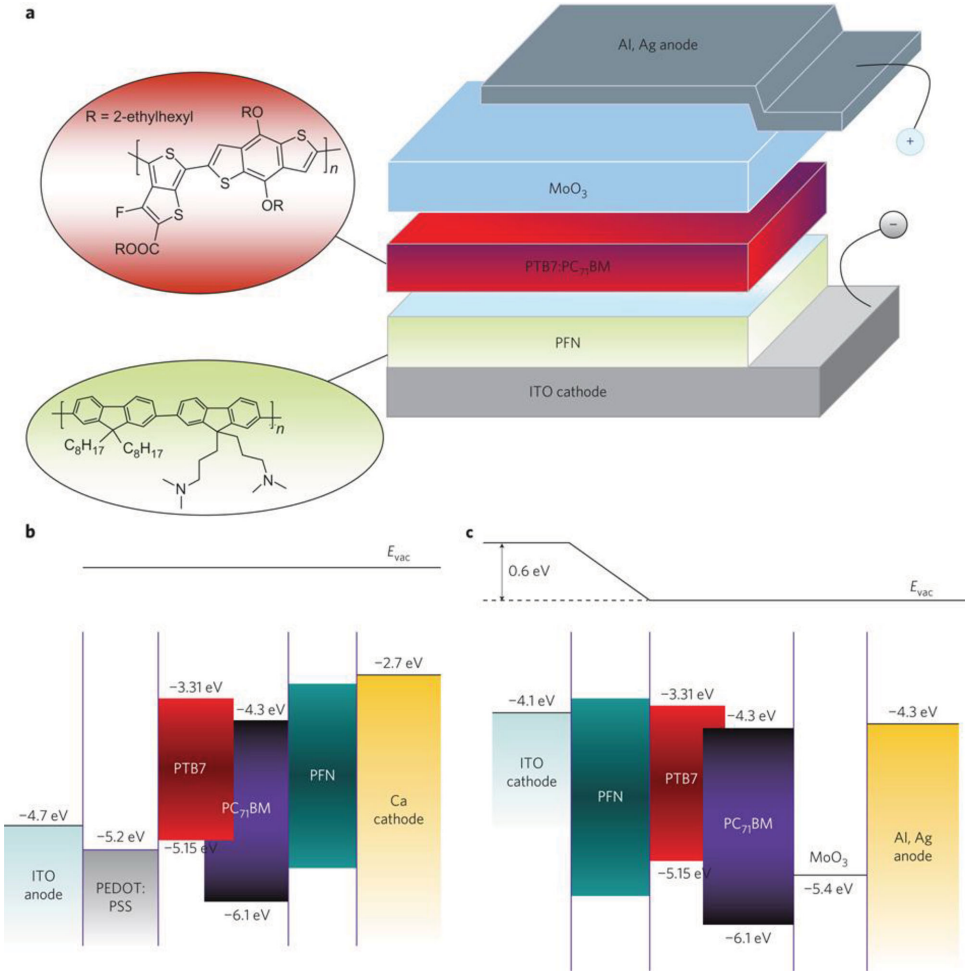

Figure 8. (a) Schematic of the inverted-type PSCs, in which the photoactive layer is sandwiched between a PFN-modified ITO cathode and an Al,Ag-based top anode. Insets: chemical structures of the water-/alcohol-soluble conjugated polymer and electron donor materials used in the study. PFN, poly [(9,9-bis(3′-(*N*,*N*-dimethylamino)propyl)-2,7-fluorene)-alt-2,7-(9,9-ioctylfluorene)]; PTB7: thieno[3,4-*b*]thiophene/benzodithiophene. (b)-(c) Schematic energy levels of the conventional (b) and inverted (c) devices under flat band conditions (open-circuit voltage). Note that the formation of a positive interface dipole moment (taking the dipole moment directed outwards to be positive) is presented in c. Reproduced with permission.[86] Copyright 2012, Nature Publishing Group.

work function of the electrodes. These work function tuning behaviors allow high work function electrodes such as ITO, silver and gold to be used as a cathode in the inverted OPV devices. Using PEIE, all-polymeric OPVs was reported having a PCE of 3.0%, with V_{oc} = 0.80 V, FF = 0.52, and J_{sc} = 7.1 mA/cm^2, which is comparable to that of a device that uses a MoO_3/Ag hole-collecting electrode (PCE of 3.5%).[87]

The device performances using the water soluble polymer were comparable to the conventional devices using evaporated charge transport layers. In addition, because water soluble polymer solutions are relatively stable in air, practical printing methods such as roll-to-roll coating method can be applied. However, the layer thickness is too thin to be fabricated by conventional printing/coating methods. Many research groups are focusing on developing ultra-thin and uniform coating technologies. The solution of such interfacial materials typically have low viscosity due to the extremely small concentration of the solid and the solvents are very different from those used for the conventional photo-active materials. Therefore, to realize the ultra-thin film of the interfacial layers, specialized coating methods are required. Only a few papers reported the results that these ultrathin layers were successfully coated. As an example, Youn et al. reported a roll-to-roll cohesive coating method as shown in **Figure 10**. Because this cohesive coating method only utilizes the cohesive force of the solution, the amount of the solution can be efficiently minimized from the nozzle. Applying such method has successfully demonstrated the devices on a relatively large scale.[88]

Besides surfactants and water soluble polymers, self-assembled monolayers (SAMs) were also widely used for electron injection materials, and Jen et al. reported that various SAMs can improve electron extraction behavior.[89–91] The process is also compatible with solution processing, and the self-assembly process naturally forms an ultra-thin layer.

3.3. Printing/Coating Technologies

The OPVs have been considered as one of the promising 3rd generation power source because they have great potential

www.MaterialsViews.com

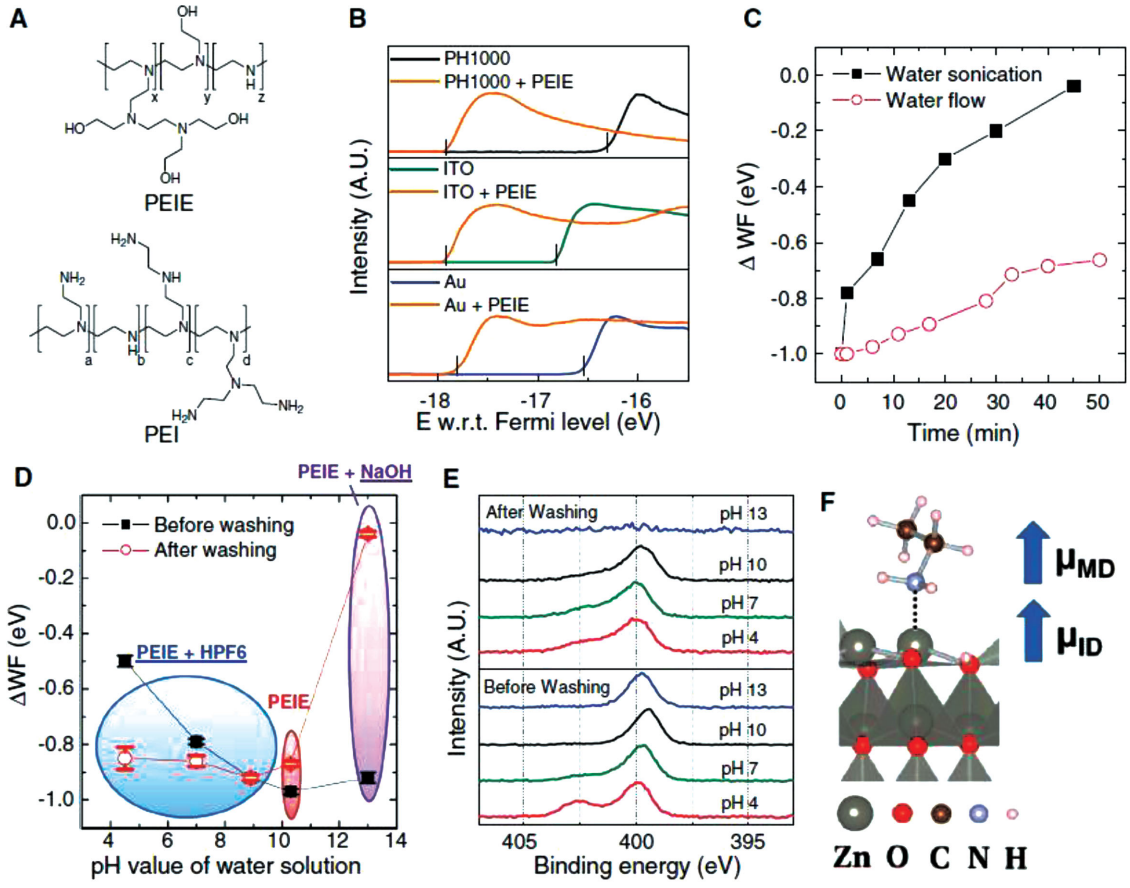

Figure 9. (a) Chemical structure of PEIE and PEI. (b) Photoemission cutoff obtained via UPS for PEDOT:PSS PH1000, ITO, and Au samples, with and without PEIE. (c) WF change, relative to bare ITO, of ITO/PEIE after different washing conditions. (d) WF change, relative to bare ITO, upon modification from PEIE water solution, PEIE with HPF_6 water solution, and PEIE with NaOH water solution before (solid squares) and after (open circles) water washing. (e) N1s core level recorded via XPS on the samples in (d) before and after washing. (f) Proposed model of molecular dipole–induced and surface dipole–induced WF reduction on ZnO surface. Reproduced with permission.[87] Copyright 2012, Science.

for the low-cost devices and scalable devices as shown in **Figure 11**. In terms of practical 1 USD$/W goal for OPVs, both of the device efficiency and manufacturing cost should be taken into account. Recently, the PCE of OPVs has been improved dramatically, and exceeded 10%.[92,93]

In terms of OPVs manufacturing, however, the materials in OPVs take up about 65–80% of the overall module cost.[94] Moreover, the estimated total module costs to produce a watt exceeds $10 as described in **Table 2**. To address this manufacturing cost issue, material waste should be minimized and sustainable and green manufacturing technologies are required. Many research groups have been investigating extensively various printing technologies such as conventional roll-to-roll printing,[95,96] inkjet printing,[97,98] screen printing,[99,100] brush painting[101,102] and spray coating[103,104] for the scalable and low-cost OPV fabrication for the past 5 years. This section deals with the issues facing the scalable and solution processed OPVs and review fabrication techniques that have been developed.

3.3.1. Traditional Roll-to-Roll Printing/Coating Process

Among conventional roll-to-roll printing processes, such as gravure, flexography and offset printing, gravure printing is a representative technique for producing the OPVs because gravure printing is appropriate for film coating and fine patterning.[105] This traditional printing process typically uses

Table 2. Optimized cost structure in terms of materials usage and processing time for the manufacturing of polymer solar cell modules. The calculation is the actual cost for the manufacture of one 16 × 13 mm module with an active area of 360 cm^2 and includes associated materials losses. Power outputs for these modules are up to 660 mW (AM 1.5 G, 1000 W/m^2). Reproduced with permission. Copyright 2010, Royal Society of Chemistry.

Material	Material cost/€	Processing cost/€	Total/€
Barrier	0.4575	0.03173	0.4892
Pressure sensitive adhesive	0.1918	0.03173	0.2236
PET-ITO	2.6077	0.21111	2.8188
ZnO	0.0582	0.16667	0.2249
P3HT-PCBM	0.4492	0.16667	0.6159
PEDOT:PSS (EL-P 5010)	0.2311	0.16667	0.3978
Silver (PV410)	0.4120	0.16667	0.5787
Total	**4.4078**	**0.9412**	**5.3491**

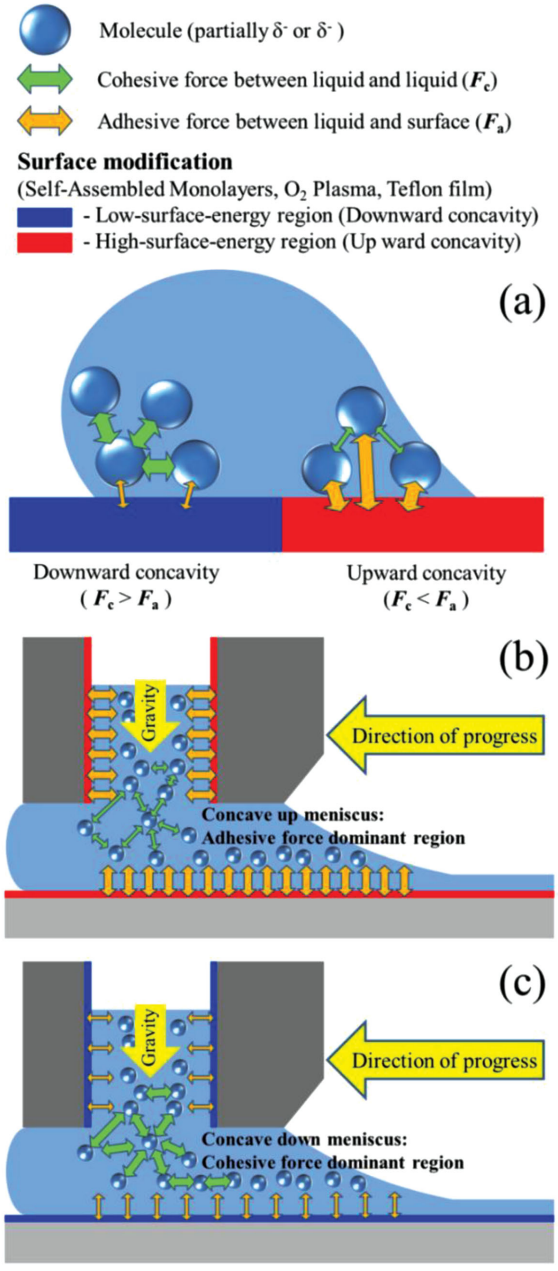

Figure 10. Illustrations of the cohesive coating mechanism and coating flows details. (a) Adhesive (Fa) and cohesive (Fc) force diagram between hydrophobic and hydrophilic surfaces. Contact angles depend on the relative forces between solvent molecules and surfaces. In the case of downward concavity, a cohesive force is higher than an adhesive force, whereas upward concavity represents that an adhesive force is higher than a cohesive force. (b) The case of adhesive force dominant condition. Adhesive forces are enhanced by surface energy modification such as O_2 plasma treatment. Therefore, the flow rate is reduced by adhesive forces. (c) The case of cohesive force dominant condition. Adhesive forces are relatively reduced by self-assembled monolayers (SAMs). Thus, the flow rate is increased. Reproduced with permission.[88] Copyright 2013, Wiley.

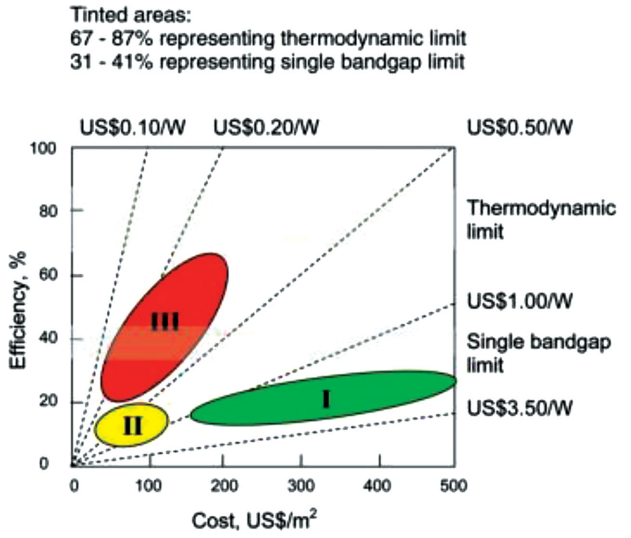

Figure 11. Efficiency and cost projections for first- (I), second- (II), and third- generation (III) PV technologies (wafer-based, thin films, and advanced thin films, respectively). Reproduced Reproduced with permission.[92] Copyright 2007, Elsevier.

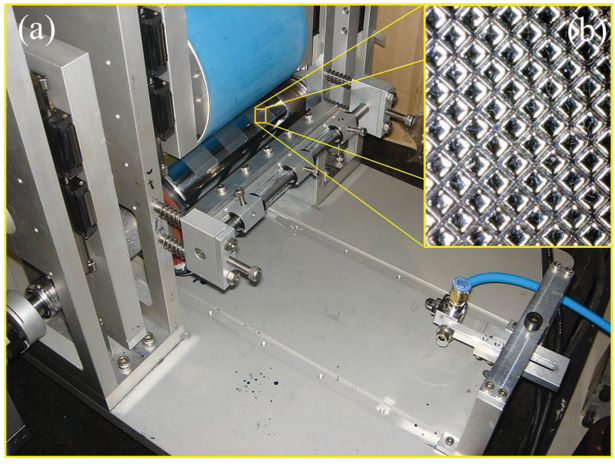

Figure 12. Picture of the gravure printing system driven by AC servo-motor. (a) 5" blanket roll (covered by blue rubber) and gravure pattern roll were contact with a printing pressure (feed back from load cell). (b) The surface on the gravure roll has tiny cells (200 line per inch) and the doctor blade (attack angle can be mechanically adjustable) was attached on the gravure roll to meter the ink.

Figure 13. Irregular coating streaks captured by high speed camera. Large molecular weight (approximately 1,000,000 molecular weight) polymer (super yellow: commercially available yellow light-emitting polymer) cases extensional viscous flow between the gravure roll and substrate, which creates unwanted streak patterns of polymer.

tiny printed dots to produce image patterns as shown in **Figure 12**b. The ink is metered by the doctor blade and contained in the micron-sized engraved cells on the surface of the printing roll. The ink is then transferred onto the substrate and then merged into a thin coating film. The gravure printing is suitable for wet-film coating process for OPV fabrication as well due to its versatilities as summarized in **Table 3**.

www.MaterialsViews.com

Table 3. The printing parameters and features in conventional roll-to-roll printing technologies.

	Screen	Gravure	Flexography	Offset
Resolution (μm)	30	20~75	75	30~50
Thickness (nm)	>1000	<50 nm	<50 nm	<1000
Viscosity (mPa·s)	500~50000	50~200	50~500	20 k~100 k
Coating Speed (m^2/s)	<10	60	10	20
Polymer ink	Fair	Excellent	Excellent	Difficult
Wet Film Coating	Difficult	Excellent	Fair	Fair

Table 4. Representative performances of the OPV devices fabricated by gravure printing process.

Structure Cathode	Gravure Printed Layers	V_{oc} [V]	J_{sc} [mA/cm^2]	FF [%]	PCE [%]	Area [cm^2]	Ref
Norm.[a] Evaporated Ca/Ag	PEDOT:PSS P3HT:PCBM	0.60	7.91	57.0	2.80	Single cell 1.9	[96]
Norm.[a] Evaporated Ca/Ag	PEDOT:PSS P3HT:PCBM	4.76	13.29	41.0	1.68	Module (8 cell) 15.45	[93]

[a]Normal structure: ITO/HTL/Active layer/Al.

However, coating issues such as non-uniform film morphology and coating instability during the gravure printing process using the functional materials of organic electronics have been discussed in several reports.[106–108] The patterns of gravure cells frequently affect the film morphologies. In particular, the organic polymers having large molecular weights create irregular coating patterns due to the extensional viscous flows as shwon in **Figure 13**. Because these coating issues may cause electrical leakage or breakage when the device is driven, we need to carefully select appropriate manufacturing technologies. Moreover, the processing conditions should be optimized such as printing speed and viscosity for the functional materials (P3HT:PCBM) as shown in **Figure 14**. The best PCE of the device fabricated by the gravure printing techniques was reported to be 2.8% in a single cell using P3HT:PCBM material system. In addition, the module efficiency of the device made by the same gravure printing system was reported 1.68% as summarized in **Table 4**. In the two cases, Ca/Ag cathode was thermally evaporated and PEDOT:PSS and P3HT:PCBM layer were gravure printed.

3.3.2. Slot-Die/Slit Coating Process

Slot-die coating or slit coating technologies are useful to realize scalable and uniform wet film in the coating industries. As we discussed above, because the conventional printing processes have coating quality issues, relatively thick active layer and PEDOT:PSS layer were fabricated by the gravure printing system. However, the slot-die coating technique is efficient to not only control the wet film thickness but also realize thinner layers such as ZnO nanoparticle layer as shown in **Figure 15**. To control the film thickness and coat uniform wet film on the substrates, homogeneous ink supplied from a static pump is important. Moreover, to obtain the thinnest film, it requires minimizing the feeding rate of the ink because the film thickness is proportion to the mass transport rate of the extruded solution. Recently, slot-die coating techniques have been widely used in OPVs and PLEDs (polymer light-emitting diodes) because the slot-die nozzle supplies constant feeding of the ink using static pumping system. For example in making PLEDs, it was found that the non-uniformities of blade-slit coated

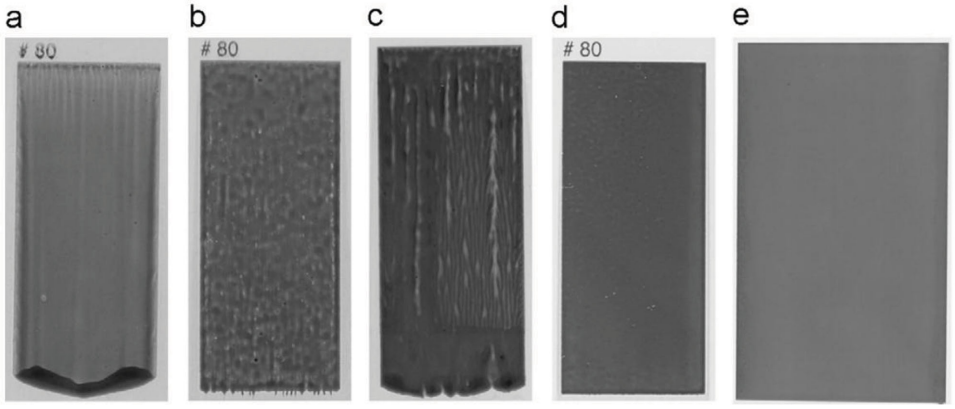

Figure 14. (a) P3HT:PCBM 50 mg/mL in o-DCB (80 l/cm), speed 7 m/min, (b) 50 mg/mL, 80 l/cm, speed 18 m/min, (c) 50 mg/mL, 45 l/cm, speed 18 m/min, (d) 100 mg/mL, 80 l/cm, speed 18 m/min, (e) 150 mg/mL, 120 l/cm, speed 18 m/min. Reproduced with permission.[108] Copyright 2010, Elsevier.

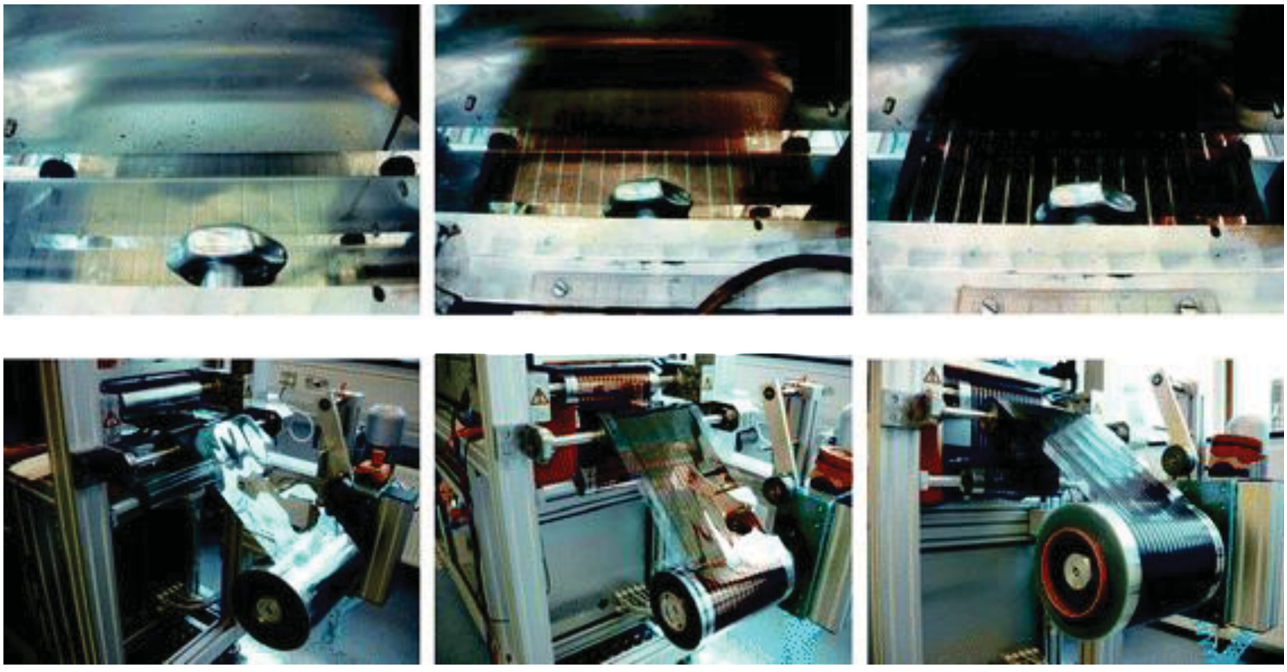

Figure 15. The slot-die coating of ZnO nanoparticles (left), P3HT:PCBM (middle) and PEDOT:PSS (right). The wet films are shown above and the corresponding dried films are shown below. Reproduced with permission.[96] Copyright 2010, Royal Society of Chemistry.

PEDOT:PSS and polymer semiconductor layer was 3.8% and 4.1%, respectively, which represents one fold improvement than that obtained by blade-only coating method (7.9% and 9.1%, respectively). The film uniformity of the slit-coated device exceeded that of the spin-coated devices (4.4–4.8%) by employing a slit nozzle on the blade.[109]

The PCE of the device using P3HT:PCBM fabricated by the slot-die coating technique was 1.96% in a inverted OPVs module. In addition, fully printed (ITO-free, screen printed back electrode) OPVs single cell using printed transparent electrode (flexography printed) was reported 1.82% as summarized in **Table 5**. In the two cases, ZnO nanoparticle layer, P3HT:PCBM and PEDOT:PSS layer were slot-die coated and Ag silver back electrodes were screen printed. In terms of green manufacturing, the slot-die coating is very promising because slot-die coating can minimize ink waste similar to the inkjet printing, but it has difficulties in arbitrary patterning. It has limitations in applying for printing complex patterns.

3.3.3. Inkjet Printing Process

Inkjet is the most common printing technique to produce digital images since it was developed from the 1950s. Because Inkjet printing can produce a wide range of free image patterns, it enables realization of metal electrodes without complex photolithography process. Though inkjet printing has great advantages in displays manufacturing such as color filters and solution processed OLEDs pixels, one need to evaluate its coating performance such as film morphologies and uniformity for printed OPVs. In the case of OPVs applications, scalable and high-throughput fabrication method is more important than fine patterning capabilities.

To fabricate the OPVs by inkjet printing system, the ink formulation (solvents and additives) should be modified to control the meniscus and ejection of the droplet from the jetting nozzle. There are much trials to apply inkjet printing in the OPVs fabrication.[110] In particular, the photo-active materials are commonly dissolved into chlorobenzen or dichlorobenzene which frequently causes printing issues as shown in **Figure 16**a. Recently, the PCE of the device fabricated by the inkjet technique was reported to 5.07% in single OPVs cell having inkjet printed PEDOT:PSS anode, PCDTBT:$PC_{70}BM$ and ZnO nanoparticle layers as shown in Figure 16c. PEDOT:PSS was modified by adding 5 wt% dimethylsulfoxide (DMSO) and 0.1% fluorosurfactant (Zonyl FS-300) to enhance the conductivity and printability.

Table 5. Representative performances in the OPVs devices fabricated by slot-die coating process.

Structure	Slot-Die Coated Layers	V_{oc} [V]	J_{sc} [mA/cm^2]	FF [%]	PCE [%]	Area [cm^2]	Ref
Inverted[a)] Flexo-printed silver mesh	ZnO NPs P3HT:PCBM PEDOT:PSS Screen printed silver	0.51	7.02	51.2	1.82	Single 6	[103]
Inverted[a)] ITO-PET	ZnO NPs P3HT:PCBM PEDOT:PSS Screen printed silver	8.47	23.2	35.4	1.96	Module(16) 15.5	[104]

[a)]Inverted structure: ITO/ETL/ Active layer /HTL/Ag.

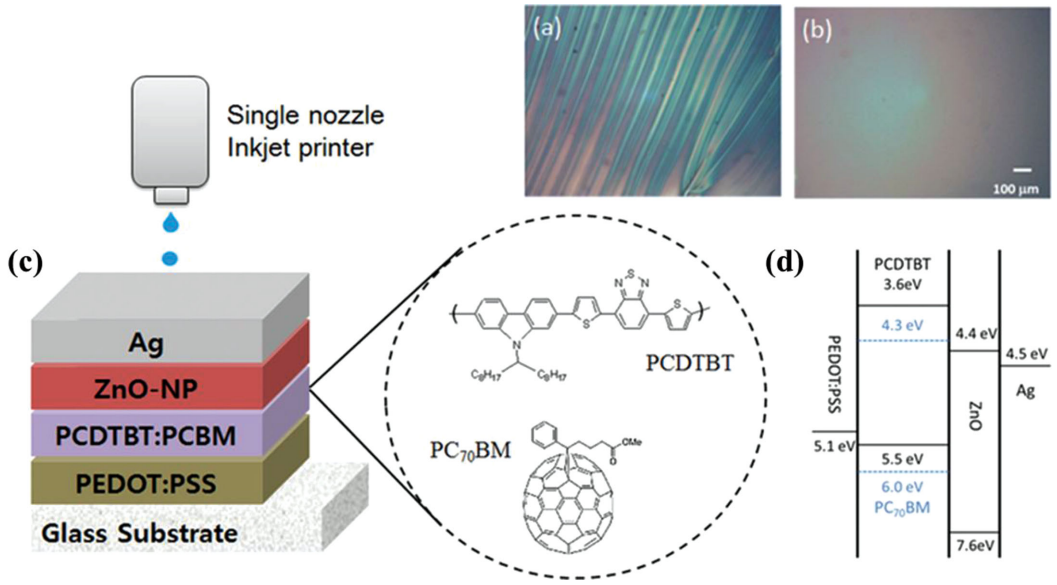

Figure 16. Microscopy images of inkjet-printed blend layers formed PCDTBT:$PC_{70}BM$ solutions (a) in chlorobenzene and (b) in a ternary solvent. (c) Device structure of an inkjet-printed solar cell and (d) energy level diagram of its components. All the four layers are printed using a single-nozzle inkjet printer and all the fabrication processes including printing, annealing and measuring have been performed in air at room temperature. Reproduced with permission.[110] Copyright 2014, Wiley.

More importantly, the top metal electrode was made by using nanoparticle based silver ink. The PCE of the all-inkjet printed OPVs was 2.05% in 0.5 cm^2 single cell as summarized in **Table 6**.

4. Fully Solution-Processed OPVs

4.1. Solution-Processed Metal Films

In fabricating OPVs, the metal electrodes are usually thermally evaporated in the vacuum chamber because they are sensitive to the moisture and oxygen in the air. Due to reasons discussed in previous sections, many researchers are investigating ways to replace the metal evaporation process by various printing technologies using the silver inks.[111,112]

The typical conductivity of the commercial grade silver paste (back electrode) is around 5×10^{-5} Ω·cm. However, because the silver pastes contain micron-scale silver flakes, they can easily penetrate and attack underlying polymer layers. To protect the few hundreds nanometer thick and soft polymer layers from the silver flakes during the printing and annealing processes, thick (1–2 μm) and highly conductive PEDOT:PSS layer was frequently inserted onto the polymer active layer.[113,114]

However, because the printed electrode using silver paste is less conductive and less reflective than the evaporated Ag film, and compounded by the light absorption by the thick PEDOT:PSS, all printed OPVs reported less than 2% PCE (best reported efficiency: 1.92%) based on P3HT:PCBM material system.[115,116] Thus, the metal film having higher and smooth surface and fabricated by solution process is highly desirable. One promising approach is to use reductive type of organometallic inks consisting of silver and organic complex. During the annealing process, the tiny silver nanoparticles (1–2 nm) are created at the initial stage and later merged into larger grains, whose sizes depend on the annealing time and temperature. To achieve better conductivity, higher annealing temperature (>180 °C) is needed to remove the residual organics and grow the silver grains inside the silver film. Such high temperature may cause thermal damages to the polymer layers and the flexible substrates. By optimizing the annealing condition and morphologies of the silver inks, the resistivity of the attained Ag film was greatly improved to 3.4 μΩ·cm as shown in **Figure 17**. On the other hand, if applied directly to the polymer semiconductor layers by solution process, the silver nanoparticles and organics very likely will infiltrate and

Table 6. Representative performances of the OPV devices fabricated by a inkjet process.

Structure	Inkjet Printed Layers	V_{oc} [V]	J_{sc} [mA/cm^2]	FF [%]	PCE [%]	Area [cm^2]	Ref
Norm.[a] Evaporated Al	PEDOT:PSS anode PCDTBT:PCBM ZnO NPs	0.82	11.55	54.3	5.07	Single 0.5	
Norm.[a]	PEDOT:PSS anode PCDTBT:PCBM ZnO NPs Ag nano-ink Printed Silver	–	–	–	2.05	Single 0.5	

[a]Normal structure: ITO/HTL/Active layer/Al.

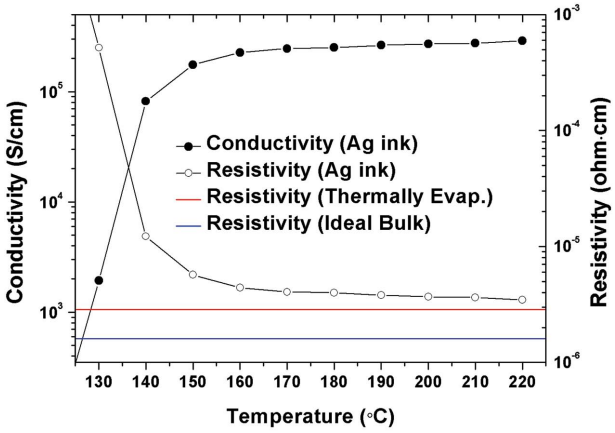

Figure 17. The conductivity and resistivity of silver film was fabricated by the reductive organometallic Ag solution. The film cast by the spin-coating then soft-baked (90 °C) and then sintered at the different temperatures (130–220 °C). The thicknesses of the Ag film were measured by the surface profilometer (Dektak) after the sintering process. The resistivity and conductivity were calculated using the parameters of the film thicknesses and sheet resistances (acquired by the 4 point prove measurement tool). The resistivity of the ideal bulk silver is 1.6 μΩ·cm. Reproduced with permission.[117] Copyright 2014, Royal Society of Chemistry.

contaminate the underlying polymer active layers, which can cause electrical failures during device operation.

4.2. Non-traditional Lamination and Transfer Methods

To overcome the penetration and contamination issues, one approach is to fabricate the solution based ink separately from the rest of the sequentially printed layer stacks. Transfer and lamination techniques could be considered to transfer the high quality metal film in solid phase. In other words, the metal films can be coated elsewhere and then transferred onto the polymer layers to complete the OPV devices. For example, as shown in **Figure 18**, multi-film roll transferring (MRT) method allows high annealing temperature and solution based fabrication process for the highly conductive and reflective film without the solvent and particle penetration issues. Moreover, this fabrication process can dramatically reduce the manufacturing time because the metal film can be prepared independently from the rest parts.

To achieve high performance in the transferred devices, the adhesion and contact among layers are very important. The adhesion between the two organic layers can be enhanced during the roller-based lamination process at elevated temperature, which is similar to that of hot pressing. The adhesion between the layer of PEDOT:PSS and P3HT:PCBM can survive the typical adhesive tape test as shown in the supplemental data section of reference paper.[117]

The power conversion efficiency of the MRT device was 3.89% using a ITO-glass substrate, slightly lower than that of the device with evaporated metal electrode due to a decrease in V_{oc} as shown in **Figure 19**. The key performance parameters including J_{sc}, V_{oc}, R_s and R_p are summarized in **Table 7**. In particular, the power conversion efficiency of the fully solution processed device (ITO free) was reported to be 3.04% using the PEDOT:PSS cathode in inverted structure (PEDOT:PSS conductive cathode/PEIE/P3HT:PCBM/PEDOT:PSS/Ag).

By using the same MRT process, a low-bandgap polymer semiconductor and fullerene: PIDT-PhanQ:$PC_{71}BM$ was used to investigate the device performance and compare the results with those made by evaporated electrode. The MRT-processed device using this low-band gap polymer showed slightly lower PCE than that of the evaporated devices due to the reduced V_{oc}, which was same issues in P3HT:PCBM. We believe that the lower V_{oc} was caused by material issues not by the fabrication method because PEDOT:PSS has lower HOMO level than that of MoO_3 as shown in **Figure 20**. However, because the fill factor is

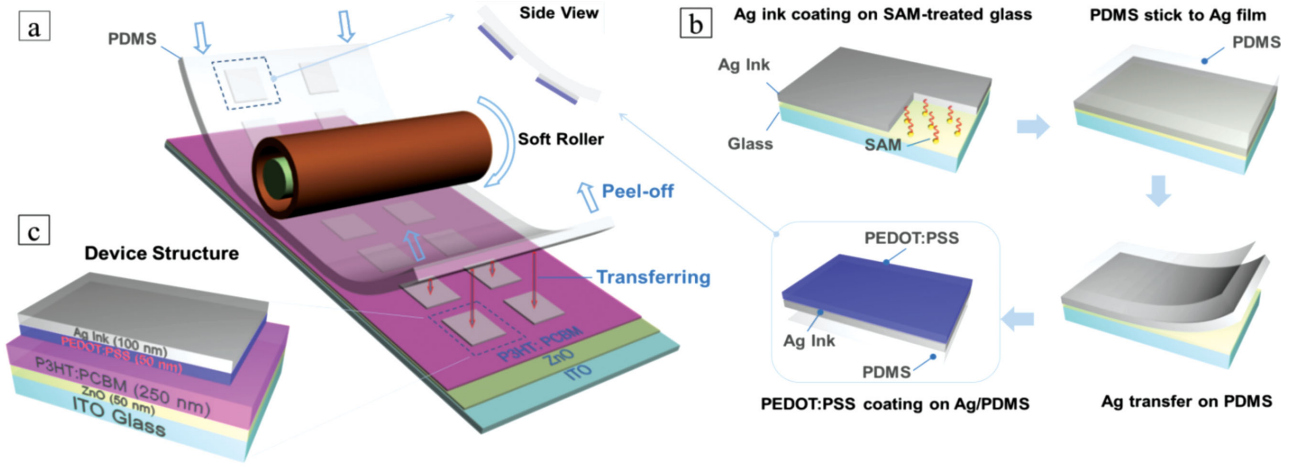

Figure 18. The illustration of the overall fabrication procedure by the multi-film roll transferring (MRT) method: (a) The highly conductive silver film cast by Ag solution and the PEDOT:PSS double layer in the flexible PDMS substrate transferred onto the photo-active layer of P3HT:PCBM with adding mild pressure by using a soft roller. (b) The silver film was coated and annealed on OTS treated glass substrate at 170 °C then the PDMS cover the silver. The silver film transfer to the PDMS and the PEDOT:PSS coated on the back side of silver film. (c) The overall device structure consisting of all-solution processed layers such as ZnO nanoparticle (electron transport layer), P3HT:PCBM (photo-active layer) and PEDOT:PSS/Ag multi-layer by the MRT process. Reproduced with permission.[117] Copyright 2014, Royal Society of Chemistry.

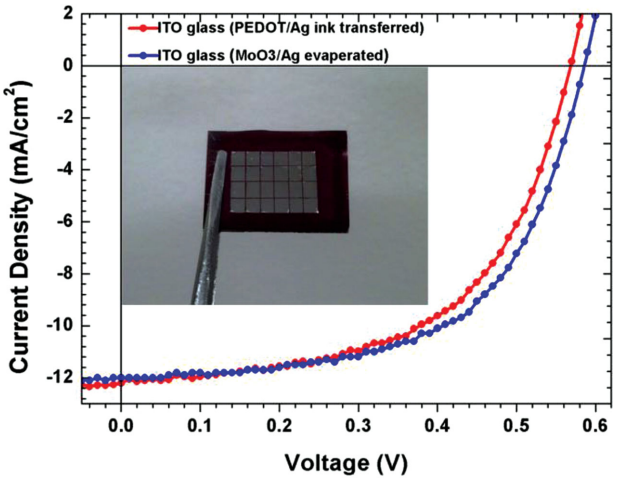

Figure 19. The *J–V* device performance of P3HT:PCBM BHJ OPVs according to the device fabrication method such as multi-film roll transferring method (MRT) or simple spin-coating. The blue line represents spin-coated device and the red one represents the device by MRT method. The inner figure in the graph showed the actual device image fabricated by MRT method, the Ag solution and PEDOT:PSS were used as reflective anode and hole transport layer respectively. Reproduced with permission.[117] Copyright 2014, Royal Society of Chemistry.

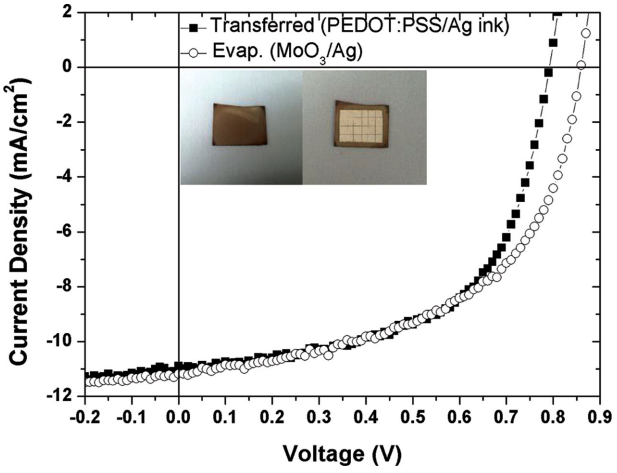

Figure 20. The *J–V* characteristics of PIDT-PhanQ:$PC_{71}BM$ OPVs made by multi-film roll transferring method (MRT) and by evaporated metal electrodes. The full device structures of the two devices are: ITO-glass/ZnO NPs/PIDT-PhanQ:$PC_{71}BM$(90 nm)/PEDOT:PSS/Ag ink (MRT), ITO-glass/ZnO NPs/PIDT-PhanQ:$PC_{71}BM$(90 nm)/MoO_3/Ag ((MRT).

better for the MRT devices and current density was comparable to the evaporated devices, the PCE (5.04%) was fairly good comparing to the evaporated device as summarized in **Table 8**.

5. Conclusion and Outlook

The high PCE (>10%) of organic photovoltaics has attracted much attention. Many researchers are focusing on approaches to control the nanomorphologies of the organic semiconductor photoactive layers, which can improve the device efficiency. However, organic photovoltaics still require innovative manufacturing technologies to realize low-cost and scalable OPVs. To achieve these goals, one needs to pay attention not only to understanding the coating properties of the functional materials, but also to developing proper fabrication methods for all functional materials. There is much to be done in order to realize OPVs as a promising power source in the future.

Table 7. The *J–V* device performance of P3HT:PCBM BHJ PSCs according to the device fabrication method such as multi-film roll transferring method (MRT), spin-coating and roll-to-roll process. Reproduced with permission.[117] Copyright 2014, Royal Society of Chemistry.

	J_{sc} [mA/cm^2]	V_{oc} [V]	FF [%]	PCE [%]	R_s[b)] [Ω cm^2]	R_p[c)] [Ω cm^2]
ITO glass + MoO_3/Ag evaporated	12.01	0.59	58.90	4.17	6.64	444
ITO glass + MRT process	12.21	0.58	54.84	3.89	7.21	401
ITO-PET + MoO_3/Ag evaporated	11.32	0.57	51.98	3.39	23.43	349
Roll-to-Roll[a)] + MRT process	9.52	0.55	57.96	3.04	24.21	443

[a)]Roll-to-roll processed device (PEDOT:PSS cathode, PEIE and P3HT:PCBM layers were roll-to-roll coated in the air atmosphere.); [b)]Series resistance; [c)]Shunt resistance.

Table 8. The electrical characteristics of the PIDT-PhanQ:$PC_{71}BM$ BHJ PSCs made by multi-film roll transferring method (MRT), spin-coating and roll-to-roll process, as compared with control devices made by evaporation.

	J_{sc} [mA/cm^2]	V_{oc} [V]	FF [%]	PCE [%]	R_s[a)] [Ω cm^2]	R_p[b)] [Ω cm^2]
MRT	10.89	0.81	58.27	5.04	4.45	300.2
Evap	11.18	0.87	53.53	5.20	6.06	424.7

[a)]Series resistance; [b)]Shunt resistance.

Acknowledgements

HSY and LJG acknowledge the partial support of the work by ONR through a subcontract from Soluxra and by NSF (DMR 1120187). HJP acknowledges partial support by the new faculty research fund of Ajou University.

The author affiliations were updated on May 20, 2015.

[1] W. S. Wong, A. Salleo, *Flexible Electronics-Materials and Applications*, Springer, Berlin **2009**.

[2] M.-G. Kang, H. J. Park, S. H. Ahn, L. J. Guo, *Sol. Energy Mater. Sol. Cells* **2010**, *94*, 1179.

[3] J. Y. Lee, T. Lee, H. J. Park, L. J. Guo, *Org. Electron.* **2014**, *15*, 2710.

[4] W. Brutting, *Physics of Organic Semiconductors*, Wiley-VCH Verlag GmbH & Co. KGaA, Weinheim, Germany **2005**.

[5] B. A. Gregg, M. C. Hanna, *J. Appl. Phys.* **2003**, *93*, 3605.
[6] B.-G. Kim, E. J. Jeong, H. J. Park, D. Bilby, L. J. Guo, J. Kim, *ACS Appl. Mater. Interfaces* **2011**, *3*, 674.
[7] M.-G. Kang, H. J. Park, S. H. Ahn, T. Xu, L. J. Guo, *IEEE J. Sel. Top. Quantum Electron.* **2010**, *16*, 1807.
[8] J. M. Halls, K. Pichler, R. H. Friend, S. C. Moratti, A. B. Holmes, *Appl. Phys. Lett.* **1996**, *68*, 3120.
[9] L. A. A. Pettersson, L. S. Roman, O. Inganas, *J. Appl. Phys.* **1999**, *86*, 487.
[10] M. Theander, A. Yartsev, D. Zigmantas, V. Sundström, W. Mammo, M. R. Anderson, O. Inganas, *Phys. Rev. B* **2000**, *61*, 12957.
[11] T. J. Savenije, J. M. Warman, A. Goossens, *Chem. Phys. Lett.* **1998**, *287*, 148.
[12] A. Haugeneder, M. Neges, C. Kallinger, W. Spirkl, U. Lemmer, J. Feldman, U. Scherf, E. Harth, A. Gugel, *Phys. Rev. B* **1999**, *59*, 15346.
[13] P. E. Shaw, A. Ruseckas, I. D. W. Samuel, *Adv. Mater.* **2008**, *20*, 3516.
[14] H. Najafov, B. Lee, Q. Zhou, L. C. Feldman, V. Podzorov, *Nat. Mater.* **2010**, *9*, 938.
[15] W. A. Luhman, R. J. Holmes, *Adv. Funct. Mater.* **2011**, *21*, 764.
[16] G. Yu, J. Gao, J. C. Hummelen, F. Wudl, A. J. Heeger, *Science* **1995**, *270*, 1789.
[17] J. J. M. Halls, C. A. Walsh, N. C. Greenham, E. A. Marseglia, R. H. Friend, S. C. Moratti, A. B. Holmes, *Nature* **1995**, *376*, 498.
[18] M. Hiramoto, H. Fujiwara, M. Yokoyama, *J. Appl. Phys.* **1992**, *72*, 3781.
[19] J. Peet, J. Y. Kim, N. E. Coates, W. L. Ma, D. Moses, A. J. Heeger, G. C. Bazan, *Nat. Mater.* **2007**, *6*, 497.
[20] J. K. Lee, W. L. Ma, C. J. Brabec, J. Yuen, J. S. Moon, J. Y. Kim, K. Lee, G. C. Bazan, A. J. Heeger, *J. Am. Chem. Soc.* **2008**, *130*, 3619.
[21] J. T. Rogers, K. Schmidt, M. F. Toney, G. C. Bazan, E. J. Kramer, *J. Am. Chem. Soc.* **2012**, *134*, 2884.
[22] F. Etzold, I. A. Howard, N. Forler, D. M. Cho, M. Meister, H. Mangold, J. Shu, M. R. Hansen, K. Mullen, F. Laquai, *J. Am. Chem. Soc.* **2012**, *134*, 10569.
[23] J. S. Moon, C. J. Takacs, S. Cho, R. C. Coffin, H. Kim, G. C. Bazan, A. J. Heeger, *Nano Lett.* **2010**, *10*, 4005.
[24] B. A. Collins, Z. Li, J. R. Tumbleston, E. Gann, C. R. McNeill, H. Ade, *Adv. Energy Mater.* **2013**, *3*, 65.
[25] M. R. Hammond, R. J. Kline, A. A. Herzing, L. J. Richter, D. S. Germack, H.-W. Ro, C. L. Soles, D. A. Fischer, T. Xu, L. Yu, M. F. Toney, D. M. DeLongchamp, *ACS Nano* **2011**, *5*, 8248.
[26] Y. M. Sun, G. C. Welch, W. L. Leong, C. J. Takacs, G. C. Bazan, A. J. Heeger, *Nat. Mater.* **2012**, *11*, 44.
[27] E. Verploegen, R. Mondal, C. J. Bettinger, S. Sok, M. F. Toney, Z. Bao, *Adv. Funct. Mater.* **2010**, *20*, 3519.
[28] W. Ma, C. Yang, X. Gong, K. Lee, A. J. Heeger, *Adv. Funct. Mater.* **2005**, *15*, 1617.
[29] B. Schmidt-Hansberg, M. Sanyal, M. F. G. Klein, M. Pfaff, N. Schnabel, S. Jaiser, A. Vorobiev, E. Muller, A. Colsmann, P. Scharfer, D. Gerthsen, U. Lemmer, E. Barrena, W. Schabel, *ACS Nano* **2011**, *5*, 8579.
[30] G. Li, V. Shrotriya, J. Huang, Y. Yao, T. Moriarty, K. Emery, Y. Yang, *Nat. Mater.* **2005**, *4*, 864.
[31] F.-C. Chen, H.-C. Tseng, C.-J. Ko, *Appl. Phys. Lett.* **2008**, *92*, 103316.
[32] F.-C. Chen, C.-J. Ko, J.-L. Wu, W.-C. Chen, *Sol. Energy Mater. Sol. Cells* **2010**, *94*, 2426.
[33] M. He, W. Han, J. Ge, Y. Yang, F. Qiu, Z. Lin, *Energy Environ. Sci.* **2011**, *4*, 2894.
[34] M. He, F. Qiu, Z. Lin, *J. Phys. Chem. Lett.* **2013**, *4*, 1788.
[35] M. He, W. Han, J. Ge, W. Yu, Y. Yang, F. Qiu, Z. Lin, *Nanoscale* **2011**, *3*, 3159.
[36] H. J. Park, M.-G. Kang, S. H. Ahn, L. J. Guo, *Adv. Mater.* **2010**, *22*, E247.
[37] H. J. Park, H. Kim, J. Y. Lee, T. Lee, L. J. Guo, *Energy Environ. Sci.* **2013**, *6*, 2203.
[38] C. W. Tang, *Appl. Phys. Lett.* **1986**, *48*, 183.
[39] N. D. Treat, M. A. Brady, G. Smith, M. F. Toney, E. J. Kramer, C. J. Hawker, M. L. Chabinyc, *Adv. Energy. Mater.* **2011**, *1*, 82.
[40] D. Chen, F. Liu, C. Wang, A. Nakahara, T. P. Russell, *Nano Lett.* **2011**, *11*, 2071.
[41] K. H. Lee, P. E. Schwenn, A. R. G. Smith, H. Cavaye, P. E. Shaw, M. James, K. B. Krueger, I. R. Gentle, P. Meredith, P. L. Burn, *Adv. Mater.* **2011**, *23*, 766.
[42] H. J. Park, J. Y. Lee, T. Lee, L. J. Guo, *Adv. Energy Mater.* **2013**, *3*, 1135.
[43] D. H. Wang, J. S. Moon, J. Seifter, J. Jo, J. H. Park, O. O. Park, A. J. Heeger, *Nano Lett.* **2011**, *11*, 3163.
[44] M. P. de Jong, L. J. van IJzendoorn, M. J. A. de Voigt, *Appl. Phys. Lett.* **2000**, *77*, 2255.
[45] F. So, D. Kondakov, *Adv. Mater.* **2010**, *22*, 3762.
[46] H. Lee, S. W. Cho, K. Han, P. E. Jeon, C.-N. Whang, *Appl. Phys. Lett.* **2008**, *93*, 043308.
[47] M. Kröger, S. Hamwi, J. Meyer, T. Riedl, W. Kowalsky, *Appl. Phys. Lett.* **2009**, *95*, 123301.
[48] E. Voroshazia, B. Verreeta, A. Buric, R. Müllera, D. D. Nuzzod, P. Heremans, *Org. Electron.* **2011**, *12*, 736.
[49] M. Vasilopoulou, L. C. Palilis, D. G. Georgiadou, S. Kennou, I. Kostis, *Appl. Phys. Lett.* **2012**, *100*, 013311.
[50] C. Tao, S. P. Ruan, G. H. Xie, X. Z. Kong, L. Shen, F. X. Meng, C. X. Liu, X. D. Zhang, W. Dong, W. Y. Chen, *Appl. Phys. Lett.* **2009**, *94*, 043311.
[51] H. Choi, B. Kim, M. J. Ko, D.-K. Lee, H. Kim, S. H. Kim, K. Kim, *Org. Electron.* **2012**, *13*, 959.
[52] T.-Y. Chu, J.-F. Chen, S.-Y. Chen, C.-J. Chen, C. H. Chen, *Appl. Phys. Lett.* **2006**, *89*, 053503.
[53] S. Han, W. S. Shin, M. Seo, D. Gupta, S. J. Moon, S. Yoo, *Org. Electron.* **2009**, *10*, 791.
[54] M. T. Greiner, M. G. Helander, W.-M. Tang, Z.-B. Wang, J. Qiu, Z.-H. Lu, *Nature. Mater.* **2012**, *11*, 76.
[55] V. Shrotriya, G. Li, Y. Yao, C. W. Chu, Y. Yang, *Appl. Phys. Lett.* **2006**, *88*, 073508.
[56] T. Stubhan, N. Li, N. A. Luechinger, S. C. Halim, G. J. Matt, C. J. Brabec, *Adv. Energy Mater.* **2012**, *2*, 1433.
[57] N. Li, T. Stubhan, N. A. Luechinger, S. C. Halim, G. J. Matt, T. Ameri, C. J. Brabec, *Org. Electron.* **2012**, *13*, 2479.
[58] J. Meyer, R. Khalandovsky, P. Görrn, A. Kahn, *Adv. Mater.* **2011**, *23*, 70.
[59] C.-P. Chen, Y.-D. Chen, S.-C. Chuang, *Adv. Mater.* **2011**, *23*, 3859.
[60] T. Stubhan, T. Ameri, M. Salinas, J. Krantz, F. Machui, M. Halik, C. J. Brabec, *Appl. Phys. Lett.* **2011**, *98*, 253308.
[61] J.-S. Huang, C.-Y. Chou, C.-F. Lin, *IEEE Electron Dev. Lett.* **2010**, *31*, 332.
[62] F. Liu, S. Shao, X. Guo, Y. Zhao, Z. Xie, *Sol. Energ. Mat. Sol. Cells.* **2010**, *94*, 842.
[63] F. Guillain, D. Tsikritzis, G. Skoulatakis, S. Kennou, G. Wantz, L. Vignau, *Sol. Energ. Mat. Sol. Cells.* **2014**, *122*, 251.
[64] S. R. Hammond, J. Meyer, N. E. Widjonarko, P. F. Ndione, A. K. Sigdel, A. Garcia, A. Miedaner, M. T. Lloyd, A. Kahn, D. S. Ginley, J. J. Berry, D. C. Olson, *J. Mater. Chem.* **2012**, *22*, 3249.
[65] K. Zilberberg, S. Trost, J. Meyer, A. Kahn, A. Behrendt, D. Lützenkirchen-Hecht, R. Frahm, T. Riedl, *Adv. Funct. Mater.* **2011**, *21*, 4776.
[66] K. Zilberberg, S. Trost, H. Schmidt, T. Riedl, *Adv. Energy Mater.* **2011**, *1*, 377.
[67] W. J. E. Beek, M. M. Wienk, M. Kemerink, X. Yang, R. A. J. Janssen, *J. Phys. Chem. B.* **2005**, *109*, 9505.
[68] K. Jeon, H. Youn, S. Kim, S. Shin, M. Yang, *Nanoscale Res. Lett.* **2012**, *7*, 253.

[69] M. He, J. Jung, F. Qiu, Z. Lin, *J. Mater. Chem.* **2012**, *22*, 24254.
[70] J. R. Manders, S.-W. Tsang, M. J. Hartel, T.-H. Lai, S. Chen, C. M. Amb, J. R. Reynolds, F. So1, *Adv. Funct. Mater.* **2013**, *23*, 2993.
[71] J. C. Wang, W. T. Weng, M. Y. Tsai, M. K. Lee, S. F. Horng, T. P. Perng, C. C. Kei, C. C. Yu, H. F. Meng, *J. Mater. Chem.* **2010**, *20*, 862.
[72] C. Y. Li, T. C. Wen, T. H. Lee, T. F. Guo, J. C. A. Huang, Y. C. Lin, Y. J. Hsu, *J. Mater. Chem.* **2009**, *19*, 1643.
[73] S. K. Hau, H. L. Yip, N. S. Baek, J. Zou, K. O'Malley, A. K. Y. Jen, *Appl. Phys. Lett.* **2008**, *92*, 253301.
[74] K. Lee, J.-Y. Kim, S.-H. Park, S.-H. Kim, S. Cho, A.-J. Heeger, *Adv. Mater.* **2007**, *19*, 2445.
[75] D. Barreraa, Y.-J. Lee, J. W. P. Hsu, *Sol. Energ. Mat. Sol. Cells.* **2014**, *125*, 27.
[76] C. Zhang, H. You, Z. Lin, Y. Hao, *Jpn. J. Appl. Phys.* **2011**, *50*, 082302.
[77] C. Wu, G. Lee, T. Pi, *Appl. Phys. Lett.* **2005**, *87*, 212108.
[78] G. Li, J. Shinar, *Appl. Phys. Lett.* **2003**, *83*, 5359.
[79] J. Huang, Z. Xu, Y. Yang, *Adv. Funct. Mater.* **2007**, *17*, 1966.
[80] X. Y. Deng, W. M. Lau, K. Y. Wonga, K. H. Low, H. F. Chow, Y. Cao, *Appl. Phys. Lett.* **2004**, *84*, 3522.
[81] T.-F. Guo, F.-S. Yang, Z.-J. Tsai, T.-C. Wen, S.-N. Hsieh, Y.-S. Fu, *Appl. Phys. Lett.* **2005**, *87*, 013504.
[82] S.-C. Chien, F.-C. Chen, M.-K. Chung, C.-S. Hsu, *J. Phys. Chem. C* **2012**, *116*, 1354.
[83] S. B. Jo, J. H. Lee, M. Sim, M. Kim, J. H. Park, Y. S. Choi, Y. Kim, S.-G. Ihn, K. Cho, *Adv. Energy Mater.* **2011**, *1*, 690.
[84] F.-C. Chen, S.-C. Chien, *J. Mater. Chem.* **2009**, *19*, 6865.
[85] F.-C. Chen, M.-K. Chuang, S.-C. Chien, J.-H. Fang, C.-W. Chu, *J. Mater. Chem.* **2011**, *21*, 11378.
[86] Z. He, C. Zhong, S. Su, M. Xu, H. Wu, Y. Cao, *Nat. Photonics* **2012**, *6*, 591.
[87] Y. Zhou, C. F. Hernandez, J. Shim, J. Meyer, A. J. Giordano, H. Li, P. Winget, T. Papadopoulos, H. Cheun, J. Kim, M. Fenoll, A. Dindar, W. Haske, E. Najafabadi, T. M. Khan, H. Sojoudi, S. Barlow, S. Graham, J.-L. Brédas, S. R. Marder, A. Kahn, B. Kippelen, *Science* **2012**, 327.
[88] S. Shin, M. Yang, L. Jay Guo, H. Youn, *Small* **2013**, *9*, 4036.
[89] H. Ma, H.-L. Yip, F. Huang, A. K.-Y. Jen, *Adv. Funct. Mater.* **2010**, *20*, 1371.
[90] S. K. Hau, H.-L. Yip, H. Ma, A. K.-Y. Jen, *Appl. Phys. Lett.* **2008**, *93*, 23304.
[91] H.-L. Yip, S. K. Hau, N. S. Baek, H. Ma, A. K.-Y. Jen, *Adv. Mater.* **2008**, *20*, 2376.
[92] G. Conibeer, *Mater. Today* **2007**, *10*, 42.
[93] J. You, L. Dou, K. Yoshimura, T. Kato, K. Ohya, T. Moriarty, K. Emery, C.-C. Chen, J. Gao, G. Li, Y. Yang, *Nat. Commun.* **2013**, *4*, 1446.
[94] S. Beaupŕe, M. Leclerc, *J. Mater. Chem. A* **2013**, *1*, 11097–11105.
[95] R. Søndergaard, M. Hösel, D. Angmo, T. T. Larsen-Olsen, F. C. Krebs, *Mater. Today* **2012**, *15*, 36.
[96] F. C. Krebs, T. Tromholt, M. Jørgensen, *Nanoscale* **2010**, *2*, 873.
[97] S. H. Eom, H. Park, S. H. Mujawara, S. C. Yoon, S.-S. Kim, S.-I. Na, S.-J. Kang, D. Khim, D.-Y. Kim, S.-H. Lee, *Org. Electron.* **2010**, *11*, 1516.
[98] C.-N. Hoth, S.-A. Choulis, P. Schilinsky, C.-J. Brabec, *Adv. Mater.* **2007**, *19*, 3973–3978.
[99] B. Zhang, H. Chae, S. Cho, *Jpn. J. Appl. Phys.* **2009**, *48*, 020208.
[100] F. C. Krebsa, M. Jørgensena, K. Norrmana, O. Hagemanna, J. Alstrupa, T. D. Nielsena, J. Fyenbob, K. Larsenb, J. Kristensenb, *Sol. Energ. Mat. Sol. Cells* **2009**, *93*, 422.
[101] S.-W. Heo, J.-Y. Lee, H.-J. Song, J.-R. Ku, D.-K. Moon, *Sol. Energ. Mat. Sol. Cells* **2011**, *95*, 3041.
[102] S.-S. Kim, S.-I. Na, J. Jo, G. Tae, D.-Y. Kim, *Adv. Mater.* **2007**, *19*, 4410.
[103] L.-M. Chen, Z. Hong, W. L. Kwan, C.-H. Lu, Y.-F. Lai, B. Lei, C.-P. Liu, Y. Yang, *ACS Nano* **2010**, *4*, 4744.
[104] S.-Y. Park, Y.-J. Kanga, S. Lee, D.-G. Kim, J.-K. Kim, J. H. Kim, J.-W. Kang, *Sol. Energ. Mat. Sol. Cells* **2011**, *95*, 852.
[105] P. Kopola, T. Aernouts, R. Sliz, S. Guillerez, M. Ylikunnari, D. Cheyns, M. Välimäki, M. Tuomikoski, J. Hast, G. Jabbour, R. Myllylä, A. Maaninen, *Sol. Energ. Mat. Sol. Cells* **2011**, *95*, 1344.
[106] J. M. Dinga, A. F. Vornbrock, C. Ting, V. Subramanian, *Sol. Energ. Mat. Sol. Cells* **2009**, *93*, 459.
[107] M. M. Voigt, R. C. I. Mackenzie, S. P. King, C. P. Yau, P. Atienzar, J. Dane, P. E. Keivanidis, I. Zadrazil, D. D. C. Bradley, J. Nelson, *Sol. Energ. Mat. Sol. Cells* **2012**, *105*, 77.
[108] P. Kopola, T. Aernouts, S. Guillerez, H. Jin, M. Tuomikoski, A. Maaninen, J. Hast, *Sol. Energ. Mat. Sol. Cells* **2010**, *94*, 1673.
[109] H. Youn, K. Jeon, S. Shin, M. Yang, *Org. Electron.* **2012**, *13*, 1470.
[110] S. Jung, A. Sou, K. Banger, D.-H. Ko, P. C. Y. Chow, C. R. McNeill, H. Sirringhaus, *Adv. Energy Mater.* **2014**, DOI: 10.1002/aenm.201400432.
[111] D. Angmo, T. T. Larsen-Olsen, M. Jørgensen, R. R. Søndergaard, F. C. Krebs, *Adv. Energy Mater.* **2013**, *3*, 172.
[112] S. K. Hau, H.-L. Yip, K. Leong, A. K.-Y. Jen, *Org. Electron.* **2009**, *10*, 719.
[113] D. Angmo, T. T. Larsen-Olsen, M. Jørgensen, R. R. Søndergaard, F. C. Krebs, *Adv. Energy. Mater.* **2013**, *3*, 172.
[114] D. Angmo, J. Sweelssen, R. Andriessen, Y. Galagan, F. C. Krebs, *Adv. Energy. Mater.* **2013**, *3*, 1230.
[115] J.-S. Yu, I. Kim, J.-S. Kim, J. Jo, T. T. Larsen-Olsen, R. R. Søndergaard, M. Hösel, D. Angmo, M. Jørgensen, F. C. Krebs, *Nanoscale* **2012**, *4*, 6032.
[116] F. C. Krebs, J. Fyenbob, M. Jørgensena, *J. Mater. Chem.* **2010**, *20*, 8994.
[117] H. Youn, T. Lee, L. J. Guo, *Energy Environ. Sci.* **2014**, *7*, 2764.

Received: September 26, 2014
Revised: November 8, 2014
Published online: January 7, 2015